NIST BUILDING SCIENCE SERIES 168

Periodic and Chaotic Motions of a Modified Stoker Column: Experimental and Numerical Results

Graham R. Cook
Emil Simiu

Center for Building Technology
National Institute of Standards and Technology
Gaithersburg, MD 20899

Issued February 1990

U.S. DEPARTMENT OF COMMERCE, Robert A. Mosbacher, Secretary
NATIONAL INSTITUTE OF STANDARDS AND TECHNOLOGY
John W. Lyons, Director

National Institute of Standards and Technology Building Science Series 168
Natl. Inst. Stand. Technol. Bldg. Sci. Ser. 168, 44 pages (Feb. 1990)
CODEN: NBSSES

U.S. GOVERNMENT PRINTING OFFICE
WASHINGTON: 1990

ABSTRACT

Records are presented of typical measured motions of a modified forced Stoker column, including periodic motion around a stable fixed point, periodic snap-through motion, and chaotic motion. Characterizations of the recorded chaotic motion include: the autocorrelation function; the spectral density plot; capacity dimensions; and the Lyapounov exponent. Two sets of numerical simulations were performed, in which the same spring stiffnesses (measured under static conditions) and the same dissipative forces (based on the viscous damping model) were used. The first set, in which the device was modeled as a multidegree of freedom system to account for the distributed mass and stiffness of the springs, yielded chaotic motions qualitatively similar to those recorded in the laboratory. No chaotic motions could be obtained from the second set, which did not reflect the fact that the spring properties are distributed and in which the device was therefore modeled as a one degree of freedom system. To the writers' knowledge this is the first reported instance of an experimental structural system with continuous members for which a qualitatively successful simulation of the chaotic motion appears to necessitate the inclusion in the model of additional degrees of freedom to account for the effects of continuity.

Key words: buckling; chaotic motion; dynamical systems; nonlinearity; structural dynamics; structural engineering; vibrations.

ACKNOWLEDGMENTS

Partial support for this work was provided by the Minerals Management Service (MMS), U.S. Department of the Interior. Charles E. Smith of the Technology Assessment and Research Branch, MMS, was Project Research Manager. The experimental device was built by Frank Rankin of the Center for Building Technology, NIST. The fractal dimension calculations were performed on the massively parallel processor of the National Aeronautics and Space Administration (NASA) by Judith E. Devaney of the Center for Computational and Applied Mathematics, NIST.

PREFACE

The nonlinear dynamic behavior of structural systems can be of concern in the design of both conventional and novel types of structures. For conventional structures, nonlinearities are principally due to inelastic material behavior in the vicinity of ultimate loads, and nonlinear dynamic analyses can be helpful in efforts to achieve realistic estimates of actual safety margins. Novel types of structures exhibiting nonlinear behavior include compliant offshore platforms, structures designed to be compliant under the effect of strong seismic loads, large orbiting structural networks, flexible robot arms, and other novel flexible or long-span structures. (Some of these structures may require passive or active controls.) In these cases nonlinearities are due to one or more of the following factors: large deformations, materials and/or joints with nonlinear behavior, and nonlinear loading.

The design of these new types of structures requires more than the ability to perform nonlinear dynamic response calculations corresponding to specified parameters and initial conditions. What is needed in addition is a qualitative understanding of the nonlinear behavior for the system at hand. Features of interest include:

(a) bifurcations, that is, changes in the character of the motion due to changes in the values of the system parameters (such as mass, damping, stiffness, wind or current speed, strength of ground motion, amplitudes and frequencies of excitation induced by waves or by control system actuators);

(b) the possible existence for any given set of parameters of two or more steady stable oscillatory forms (attractors), each with its corresponding set of initial conditions (basin of attraction);

(c) jumps from one oscillatory form to another that can occur in bi- or multi-stable systems;

(d) the possible existence of motions that are sensitive to initial conditions and therefore cannot, in practice, be predicted numerically for sufficiently long times, since this would require virtually error-free initial conditions and computational algorithms (these motions are referred to as chaotic).

Examples of bifurcations in structural dynamics problems include: the onset of the critical flutter speed (corresponding to a Hopf bifurcation, also referred to by some mathematicians as the Poincare-Andronov bifurcation, i.e., a bifurcation from a fixed point to periodic motion); and bifurcations from periodic or quasiperiodic to chaotic motion for certain types of offshore structures [1-3], for single forced or coupled autonomous galloping oscillators [4], or for forced circular cylinders excited by vortices shed in their wake [5].

As pointed out in recent studies of nonlinear and chaotic motions of compliant offshore structures reported in [1-3], the design of nonlinear structures can be grossly inadequate or even disastrous if the analyst fails to account for the diversity of possible types of responses that may correspond to (a) various sets of system parameters, or (b) a given set of system parameters and various sets

of initial conditions. Even before the advent of compliant platforms such failures have occurred: the design of the old Tacoma Narrows bridge, which collapsed in 1940, is one example. In this case the possibility of an aeroelastic instability, that is, of a Hopf (Poincare-Andronov) bifurcation apparently did not even occur to its designers.

The solution of nonlinear structural engineering problems such as those mentioned earlier requires approaches that depend in a fundamental way upon the quality of physical modeling. For example, in spite of the availability of the requisite mathematical tools that had previously been developed for the analysis of airfoil flutter, aeronautical experts -- including von Karman -- were unable to calculate the critical flutter speed for the old Tacoma Narrows bridge until it was recognized three decades later that aerodynamic lift forces and moments derived for airfoils are inapplicable to bluff shapes [6]. However, intertwined with questions of physical modeling are mathematical questions that can be of great difficulty, so that the engineer needs whatever nonlinear mathematics relevant to his problem is available (and usually more). These questions become more difficult when the nonlinearities are strong, as is the case when they are induced by hydrodynamic -- as opposed to aerodynamic -- effects.

The assimilation and stimulation by structural engineers of mathematical developments applicable to previously unknown types of structures goes far back in the history of structural engineering. The development by Euler of the theory of elastic stability occurred in time to help designers of steel and cast iron columns avoid the need for costly lessons through disastrous structural failures. We have already mentioned the old Tacoma Narrows bridge, whose designers were less fortunate, since no aeroelastic theory applicable to bridges was available to them.

In view of forthcoming developments in the design of structures with nonlinear behavior, including structures with passive or active controls, it appears reasonable to create a body of structural engineering knowledge drawing on recent progress -- and with the potential for stimulating further progress-- in nonlinear dynamical systems theory. For this reason, the Center for Building Technology and the Center for Computational and Applied Mathematics of the National Engineering Laboratory, National Institute of Standards and Technology, are engaged in a cooperative effort the ultimate goal of which is to facilitate the application by structural engineers of methods developed within the framework of nonlinear dynamical systems theory. The first phase of this effort is aimed at studying the experimental, numerical and analytic behavior of two structural systems chosen for their relative simplicity and for their capability to exhibit chaotic motions for certain ranges of system parameters. The writers believe that these systems offer a useful opportunity for familiarization with existing tools used in dynamical systems theory, and the potential for gaining useful insights into the behavior of real systems susceptible of experiencing chaotic motion. One type of system, briefly described in [4], is fluidelastic in nature and consists of galloping oscillators, either single and harmonically forced, or coupled and autonomous. This system is of potential interest in power line engineering and in ocean engineering applications involving cables with marine growth. A second type of system, consisting of a structural member buckled under compression and subjected to periodic forcing, is described in the present report.

LIST OF SYMBOLS

a = propagation velocity
A = amplitude of forcing arm motion
c = viscous damping coefficient
F = force
F_1, F_2 = forces defined in figure 4.1
g, g_1, g_2, $g_{\theta 1}$, $g_{\theta 2}$, g_{1i} = dissipative forces
h_{1i}, h_{2i} = dissipative forces
k = spring constant
k_1, k_2 = stiffness of left and right horizontal spring, respectively
K_1 = total stiffness of torsional springs
K_2 = total stiffness of vertical springs
ℓ = half of total column length
L = spring length
m = mass assumed to be concentrated at column midpoint (fig. 2.1)
M = sum of mass m and tributary masses of horizontal springs
m_{h1}, m_{h2} = total mass of left and right horizontal spring, respectively
m_v = total mass of vertical spring
m_1, m_2 = mass assumed to be concentrated at upper and lower column support
M_1 = sum of mass m_1 and tributary mass of vertical spring
M_2 = sum of mass m_2 and tributary mass of vertical spring
N = capacity dimension
n_h = number of segments into which horizontal springs are divided
n_v = number of segments into which vertical springs are divided
P_o = total tension in vertical springs corresponding to $x = 0$
P_{1i}, P_{2i} = vertical spring forces (figs. 4.1 and 4.2)
R_{1o}, R_{2o} = tensions in left and right horizontal springs corresponding to zero displacements of mass m and of the forcing arms
R_{1i}, R_{2i} = horizontal spring forces (figs. 4.1 and 4.3)
t = time
T = torsional moment (fig. 4.1)
t_o = ratio t/τ
t_p = disturbance propagation time
V_{11}, V_{21} = forces defined in figure 4.1
w = nondimensional displacement in Duffing equation
x = displacement of mass m
x_o = ratio x/w
x_{1i}, x_{2i} = displacements of lumped masses of left and right horizontal spring segments (fig. 4.2)
y_{1i} = displacements of lumped masses of vertical spring (fig. 4.3)
z_i = auxiliary coordinates
$-\alpha$, β = coefficients of linear and cubic term, respectively, in eq (4.34)
γ = Lyapounov exponent
$\delta(x)$ = displacement of mass m_1 and of mass m_2
ϵ = strain
θ = angle defined by figure 4.1 and eq (4.12)
ρ = mass per unit length
τ = nondimensionalized time
ω = frequency forcing arms motion
Ω = nondimensionalized frequency of forcing arms motion
$'$ denotes differentiation with respect to time

CONTENTS

	Page
Abstract	iii
Acknowledgments	iv
Preface	v
List of symbols	vii
1. Introduction	1
2. Description of Experimental Device	2
3. Experimental Results	3
4. Analytical Modeling	5
4.1 Modeling of Spring Masses and Stiffnesses	5
4.2 Modeling of Dissipative Forces	6
4.3 Equations of Motion	6
4.3.1 Equations of Motion of Multidegree of Freedom System	7
4.3.2 Single Degree of Freedom System	8
4.3.3 Duffing Equation	9
5. Numerical Simulations	10
5.1 Numerical Simulation of Observed Chaotic Motion	10
5.2 Effect of Simplified Representation of the Device as a One Degree of Freedom System	11
6. Summary and Conclusions	12
7. References	12

List of Figures

Figure 2.1.	Schematic of Forced Modified Stoker Column	14
Figure 2.2.	Drawing of Forced Modified Stoker Column	15
Figure 2.3.	Photograph of Forced Modified Stoker Column	16
Figure 3.1a.	Time History of Displacement x	17
Figure 3.1b.	Time History of Displacement x	18
Figure 3.1c.	Time History of Displacement x	19
Figure 3.2.	Time History of Displacement x	20
Figure 3.3.	Phase Plane Diagram	21
Figure 3.4.	Intersections of Orbit x, x', t with Planes $t=2\pi n/\omega$ ($n = 1,2,...$)	22
Figure 3.5.	Mapping of Successive Local Maxima of x, x_i versus x_{i+1}	23
Figure 3.6.	Spectral Density Function of x	24
Figure 3.7.	Autocorrelation Function of x	25
Figure 3.8.	Snap-through Oscillations	26
Figure 3.9.	Spectral Density of Snap-through Oscillatory Motion	27
Figure 3.10.	Oscillations Around a Stable Fixed Point of the Unforced Motion	28
Figure 3.11.	Spectral Density of Oscillatory Motion Around Fixed Point	29
Figure 4.1.	Free Body Diagrams	30
Figure 4.2.	Lumped Masses Representing Vertical Springs ($n_v = 4$)	31
Figure 4.3.	Lumped Masses Representing Horizontal Springs ($n_h = 4$)	31
Figure 4.4.	Dependence of Potential Function on Displacement $\|x\|$ for One Degree of Freedom System	32
Figure 5.1.	Time History of Simulated Chaotic Motion	33
Figure 5.2.	Stroboscopic Poincare Plot of Simulated Chaotic Motion	34
Figure 5.3.	Spectral Density Plot of Simulated Chaotic Motion	35

1. INTRODUCTION

The purpose of this report is twofold. First, it describes an experimental device designed to demonstrate periodic and chaotic behavior of a buckled column subjected to harmonic forcing. Second, it attempts to reproduce the behavior of the system numerically using relatively simple analytical models comparable to those that might be used in engineering practice. Comparisons between models with various degrees of complexity are made, which provide some insight into issues related to analytical modeling for structures that can experience chaotic behavior. The work presented here can be viewed as the first phase of a broader experimental, analytical, and numerical investigation into the behavior of the forced buckled column, which would explore additional issues of engineering interest. The conditions under which noise can change dynamic behavior qualitatively are one such issue. Another issue is the occurrence of chaotic behavior when the excitation, rather than being periodic, is due to the superposition of two harmonics (a topic investigated theoretically for certain simple systems in [7]), or to a relatively large number of harmonics that mimic a stochastic process such as excitation by waves.

The experimental device was designed to exhibit clearly the physical mechanisms underlying its excitation and response and -- to within unavoidable noise effects -- the deterministic nature of those mechanisms. Its predecessors are a pioneering magnetoelastic analog [8] and an electrical analog [9] of a buckled column. However, our device is strictly mechanical and actually consists of a physical column subjected to compressive loads that cause it to be buckled at all times.

In view of the similarity of the device of [8], it was judged that the device has the capability of exhibiting chaotic behavior, in spite of its structurally more complex nature, which will be examined subsequently.

A Stoker column is an ideally frictionless buckled column with constant compressive load and with mass and bending stiffness concentrated at its midpoint [10, p. 54]. A Stoker column with energy dissipation, forced periodically at its midpoint in a direction normal to the load, can exhibit chaotic behavior for certain parameter ranges [8,11]. Practical difficulties associated with the constancy of the compressive load appear to have prevented so far the construction of such a device. The interesting motions associated with the forced, dissipative Stoker column are due to the presence of a homoclinic point at the origin of the phase plane diagram for the corresponding unforced, Hamiltonian (nondissipative) system. However, the compressive load need not be constant for such motions to occur. The dissipative forced Stoker column was therefore modified as follows. The compression forces are supplied by prestressed springs connected to the column ends. Since the elongations of those springs vary during the forced motion of the column, so do the compression forces. In addition, for reasons of construction, the modified column also has concentrated masses at its ends. Finally, the springs have considerable mass, so that the system being considered is continuous, i.e., it has an infinite number of degrees of freedom. The device so constructed is referred to here as the modified Stoker column.

Section 2 of the report contains a description of the experimental device. Section 3 presents descriptions of column motions, including time histories, phase plane diagrams, Poincare plots, spectral density functions, and autocorrelation functions. Estimates of fractal (capacity) dimensions and of Lyapounov exponents characterizing the motion are also included. Section 4 briefly discusses analytical models used for the modified Stoker column and includes the derivation of corresponding equations of motion. Section 5 includes results of numerical simulations based on various analytical models and discusses their adequacy in light of the experimental results. Section 6 consists of a summary and conclusions.

2. DESCRIPTION OF EXPERIMENTAL DEVICE

A schematic of the device is shown in figure 2.1. The column is assumed to have three concentrated masses; a mass m at its midpoint, a mass m_1 at its top end, and a mass m_2 at its bottom end. Torsional springs at the midpoint supply the total concentrated bending stiffness K_1. The column is tied at its ends by vertical springs with total mass m_v and total stiffness K_2. The column ends and the masses attached to them are free to slide vertically but are constrained in the horizontal direction. The mass m is free to slide horizontally but is constrained in the vertical direction. This ensures the symmetry of the column motion with respect to the horizontal line passing through the column midpoint. The mass m is tied by two springs, with masses m_{h1} and m_{h2} and stiffnesses k_1 and k_2, to two rigid arms forced by a motor to move harmonically (with amplitude A and circular frequency ω) and in phase in the horizontal direction. A drawing and a photograph of the device are shown in figures 2.2 and 2.3.

Each column consists of a pair of identical members. Each member is equipped with a vertical spring and with two torsional springs. This arrangement, similar to that of a tied arch discussed in [12, p. 55], allows the occurrence of snap-through oscillations. Friction between the moving mass m and its horizontal guides was reduced by providing the mass with roller bearing guide wheels. The columns are connected at their ends to horizontal axles sliding within vertical guides. To reduce friction the vertical guides are lined with teflon, and the ends of the axles are provided with teflon pads. The connections of the ends of the columns to the axles was done through roller bearings. The vertical springs are connected to the bottom axles by S-hooks positioned onto the axles by clip rings. The top ends of the vertical springs are suspended from the lower eye of turnbuckles whose upper eye rests on the axles. The turnbuckles allow the adjustment of the pretension in the springs. The rigid arm to which mass m is connected by the horizontal springs is driven at the desired frequency by a low inertia servomotor with tachometer feedback. Measurements indicated that the frequency varies in time by as much as 1% of its mean value. The amplitude of the forced rigid arm motion can also be adjusted as needed within the range 0.02 to 0.035 m. Displacements of the mass m are measured using a single turn precision potentiometer with a ball bearing mounted shaft and a linearity of 0.05%.

All springs were manufactured from chromium silicon steel, which was selected for its superior fatigue performance. Both vertical and horizontal springs behave linearly under static testing (i.e., low loading rate) except near the

origin of the force-displacement diagram. The undeformed length of the vertical springs was 0.18 m; their outside diameter 0.01667 m; the wire diameter was 0.002324 m; and the inside diameter of the hooks was 0.0096 m. The total mass of the two vertical springs, m_v, was 0.234 kg. The undeformed length of the horizontal springs was 0.1825 m; the outside diameter was 0.01429 m; the wire diameter 0.0015875 m; and the inside diameter of the hook was 0.0873 m. The mass of each horizontal spring, $m_{h1} = m_{h2}$ was 0.07 kg. Within the linear range, the spring stiffnesses were $K_2 = 2{,}640$ N/m for the vertical springs and $k_1 = k_2 = 264$ N/m for the horizontal springs.

The springs are pretensioned so as to be under tension and linear at all times. The spring extensions corresponding to x = 0 were 30 mm for the vertical springs. For the horizontal springs, when the displacements of the forcing rigid arms were equal to zero, the spring extensions corresponding to x = 0 were 80 mm.

The torsional springs, as mounted on the vertical shaft located at the midheight of the columns, are linear under static testing over the range of angular deformations 0 - 0.336 radians ($|x| < 0.066$ m), their total stiffness within this range being $K_1 = 10.9$ Nm/rad. For angular deformations larger than 0.336 radians ($|x| > 0.066$ m) the torsional springs behave nonlinearly, and measurements under static testing yielded the approximate relation

$$K_1(x) = (27015.3\ |x| - 1772.1)\ \text{Nm/rad} \qquad (|x| > 0.066\ \text{m}). \qquad (2.1)$$

The design of the experimental device makes it possible to change the springs, the masses, and the amplitude and circular frequency of the horizontal forcing motion. The total length of the column, however, is fixed ($2\ell = 0.4$ m).

3. EXPERIMENTAL RESULTS

The properties of the system for which the experimental results presented in this section were obtained were:

$\ell = 0.200$ m
$m = 0.490$ kg
$m_1 = 0.155$ kg
$m_2 = 0.128$ kg
$A = 0.02425$ m

The forcing frequency was varied as described below. The spring properties were those given in section 2. Mass m as given above includes, in addition to the mass attached to the column midpoint, the tributary mass of the columns themselves and the total mass of the torsional springs (0.084 kg). Masses m_1 and m_2 consist of the tributary mass of the columns themselves, the spring attachments and the mass of the column axles.

We show in figures 3.1a, 3.1b, and 3.1c a 300 s time history (x, t) of steady state motion corresponding to the properties just listed. For comparison with subsequent figures we also show at an expanded scale in figure 3.2 the time

history for the first 40 s of figure 3.1a. The forcing frequency for the motions of figures 3.1 and 3.2 was $\omega = 37.315$ rad/s.

Figure 3.3 shows the phase plane diagram (x, x′) corresponding to figure 3.2.

Figure 3.4 shows the points obtained by intersecting the trajectory (x, x′, t) with planes $t = 2\pi n/\omega$ (n = 1, 2,...), where ω is the nominal forcing frequency. (The velocities x′ were estimated from the recorded time series x.) This diagram would be a stroboscopic Poincare plot if the nominal and actual forcing frequency were the same. As indicated in section 2, however, the actual frequency varies by as much as 1% of its mean value. The plot of figure 3.4 is therefore affected by errors associated with this variation.

Figure 3.5 shows a different Poincare plot which is not susceptible of experiencing such errrors. It was obtained by using the surface of section x′ = 0 and therefore represents the mapping of the local maxima of the displacement, x_{i+1}, versus their immediate antecedents, the local maxima x_i. If the motion were periodic or quasiperiodic, this plot would consist, respectively, of a finite number of points or of a dense set of points on a closed curve. The plot of figure 3.5 appears, however, to be a fractal object. This was confirmed by calculations of its capacity dimension [13, 14], which was estimated to be 1.25. The estimate was based on about 2000 points from figure 3.5 (corresponding to a record approximately 300 s long). It was performed by Judith E. Devaney of the Center for Computational and Applied Mathematics, NIST, using the procedure developed by Sullivan and Hunt in [15].

The spectral density of the displacement is represented in figure 3.6. The broadband components of the spectrum are noted. To a broadband spectrum there corresponds a decaying autocorrelation function, as seen in our case in figure 3.7. The decay and the vanishing (to within noise effects) of the autocorrelation function reflects the unpredictability of future motions given a known time history. Thus, the broadband character of the spectrum is an indication that the motion is chaotic.

For the three-dimensional attractor of the system the capacity dimension was estimated to be 2.3. This estimate was based on the three-dimensional time-dependent vector obtained by embedding the time series of the response, x(t), in a three-dimensional space as follows. The first coordinate of the vector was x(t) itself. The second and the third coordinates were $x(t + \tau)$ and $x(t + 2\tau)$, respectively, where the delay time $\tau = 0.6425$ s is the time lag corresponding to the first zero of the autocorrelation function shown in figure 3.7 (see, e.g., [13]). The estimate was performed for a first set of 65,000 points obtained in this fashion, and corresponding to the first half of 300 s long record. The estimated capacity dimension based on the second half of that record was also 2.3. These estimates were also performed by J. E. Devaney using the procedure of [15].

The Lyapounov exponent was estimated using the procedure described in [16]. The computer program for implementing the procedure was made available to the writers by Professor A. Wolf. For embedding dimensions D = 2 and 3 we obtained estimates of the Lyapounov exponents corresponding to input parameters appropriate to our problem (SCALMIN = 0.002 m, SCALMAX = 0.01 m, EVOLV = 500,

see [16, p. 313]). The estimated values were γ = 2.99 bits/s for D = 2, and γ = 3.14 bits/s for D = 3. For higher embedding dimensions noise effects appeared to affect the results significantly, although the estimated Lyapounov coefficients remained positive and of the same order of magnitude up to D = 7.

The forcing frequency was then changed from ω = 37.315 rad/s to ω = 22.702 rad/s, while all other parameters were left unchanged. A periodic snap-through motion was recorded, as shown in figure 3.8. Figure 3.9 shows the corresponding spectral density function. The presence of noise is clearly reflected in figure 3.9, but its level is considerably lower than that of the broadband components of the chaotic motion shown in figure 3.6.

Finally, we show in figure 3.10 the time history of periodic motion about a stable fixed point of the unforced column. This occurred for a forcing frequency ω = 22.800 rad/s, all other system parameters being unchanged. It is noteworthy from an engineering standpoint that the behavior of the system is radically different from that of figure 3.8 even though the respective frequencies differ by less than 0.5%. The spectral density of the motion of figure 3.10 is shown in figure 3.11.

4. ANALYTICAL MODELING

4.1 Modeling of Spring Masses and Stiffnesses

The system under consideration is continuous, i.e., it has an infinite number of degrees of freedom. This is due to the relatively significant mass of the horizontal and vertical springs.

For a linearly elastic member in tension the propagation velocity for a disturbance is $a = [(F/\epsilon)/\rho]^{1/2}$, where F = force acting on member, ϵ = strain induced by force F, and ρ = mass of member per unit length. For a linear spring with total mass m_s and length L to which there corresponds a spring constant k, F = k, ϵ = 1/L, $\rho = m_s/L$, and $a = (k/m_s)^{1/2}L$. The time required for the propagation of a disturbance from one end of a spring to the other is $t_p = L/a$, and the length, spring constant and mass are approximately 0.18 m, 2640 N/m, and 0.234 kg for the vertical springs, and 0.18 m, 265 N/m, and 0.07 kg for each of the horizontal springs. Therefore, the propagation times are about 0.01 s and 0.016 s, respectively. These times should be compared with a quarter of the forcing period (i.e., the time required for the forcing arm displacement to go from zero to its maximum value), which for the chaotic oscillations is $2\pi/37.315$ = 0.042 s, that is, only a few times larger than the propagation times. This suggests that the continuity of the system due to the masses of the horizontal and vertical springs may be a significant factor in the modeling of the experimental device.

An additional modeling issue is whether the spring stiffnesses as measured under static conditions are applicable to dynamic conditions. Given the constraints of the project dynamic testing could not be performed, and it was assumed in the simulations that the spring stiffnesses under static and dynamic conditions are the same. However, we believe that the modeling of the system might have been

improved if the spring stiffnesses had been carefully measured under dynamic conditions, particularly for the as-mounted torsional springs.

4.2 Modeling of Dissipative Forces

Energy dissipation is due to both internal friction in the springs and to friction between moving parts of the device, including in particular the friction of the torsional springs against the shaft onto which they are mounted. The measurement of the dissipative forces was beyond the scope of this work. Some of these forces are nonlinear, and our observations indicated that this is in particular the case for the dissipative forces associated with the torsional spring forces $|x| > 0.066$ m. Nevertheless, in simulating the motions we used the simplified assumption that the total damping is proportional to the velocity x' of the column midpoint, the factor of proportionality being a constant viscous damping coefficient. We also carried out simulations in which we assumed that the viscous damping coefficient was constant for $|x| < 0.066$ m and increased linearly for $|x| > 0.066$ m. The results of our simulations will be commented upon in light of the limitations of these simplified models.

4.3 Equations of Motion

The equations of motion can be derived by considering the free body diagram for masses M, M_1 and M_2, where M is the sum of mass m and the tributary masses of the horizontal springs, and M_1 (M_2) is the sum of mass m_1 (m_2) and the tributary mass of the vertical spring. The motion of masses m_1 and m_2 is constrained; denoting their displacements by $\delta(x)$ we have (fig. 2.1):

$$\delta(x) = \ell - (\ell^2 - x^2)^{1/2} \ . \tag{4.1}$$

Let the differentiation with respect to the time t be denoted by '. It follows from figure 4.1 that

$$V_{11} = P_{11}(x) + M_1\, \delta''(x) + g_1 \tag{4.2}$$

$$V_{21} = P_{21}(x) + M_2\, \delta''(x) + g_2 \tag{4.3}$$

$$-\frac{T}{2} + V_{11}\, \ell \sin\theta - F_1\, \ell \cos\theta - g_{\theta 1} = 0 \tag{4.4}$$

$$-\frac{T}{2} + V_{21}\, \ell \sin\theta - F_2\, \ell \cos\theta - g_{\theta 2} = 0 \tag{4.5}$$

$$M\, x'' + g - F_1 - F_2 - R_{11} + R_{21} = 0 \tag{4.6}$$

where g, g_1, g_2, $g_{\theta 1}$, $g_{\theta 2}$ denote the dissipative forces (moments). For the reader's convenience we note that

$$\delta'(x) = xx'/(\ell^2 - x^2)^{1/2} \tag{4.7}$$

$$\delta''(x) = [1/(\ell^2 - x^2)^{1/2}]\, [xx'' + x'^2 + x^2x'^2/(\ell^2 - x^2)] \ . \tag{4.8}$$

4.3.1 Equations of Motion of Multidegree of Freedom System

To account for the forces of inertia associated with the mass of the springs, we divide the springs into segments, each having a lumped mass and stiffness. If we divide the vertical springs into n_v equal segments, the mass and the stiffness of each segment will be m_v/n_v and n_vK_2, respectively, where m_v and K_2 are, respectively, the mass and the stiffness of the original undivided spring. A tributary mass $m_v/(2n_v)$ will be added to the top mass m_1 as well as to the bottom mass m_2. Similar statements hold for the horizontal springs, which are each divided into n_h segments. We will assume for convenience that n_v and n_h are even.

The system of eqs (4.1) through (4.6) must then be complemented by the equations of motion of the spring segments. Owing to symmetry, $P_{21}(x) = P_{11}(x)$, and we need to write only the equations of motion of the upper $n_v/2 - 1$ lumped masses of the vertical springs (fig. 4.2):

$$\frac{m_v}{n_v} y_{1i}'' + g_{1i} - P_{1i} + P_{1i+1} = 0 \qquad (i = 1, 2, ..,n_v/2 - 1) . \qquad (4.9)$$

For the horizontal spring segments (fig. 4.3):

$$\frac{m_{h1}}{n_h} x_{1i}'' + h_{1i} + R_{1i} - R_{1i+1} = 0 \qquad (i = 1, 2, ..,n_h - 1) \qquad (4.10)$$

$$\frac{m_{h2}}{n_h} x_{2i}'' + h_{2i} - R_{2i} + R_{2i+1} = 0 \qquad (i = 1, 2, ..,n_h - 1) \qquad (4.11)$$

where g_{1i}, h_{1i}, h_{2i} denote the dissipative forces. The forces in the springs are

$$P_{11} = P_o - n_vK_2 [\delta(x) + y_{11}] \qquad (4.12)$$

$$P_{1i} = P_o + n_vK_2 (y_{2i-1} - y_{1i}) \qquad (i = 2,3,..,n_v/2 - 1) \qquad (4.13)$$

$$R_{11} = R_{1o} + n_hk_1(x_{11} - x) \qquad (4.14)$$

$$R_{1i} = R_{1o} + n_hk_1(x_{1i} - x_{1i-1}) \qquad (i = 2,3,..,n_h - 1) \qquad (4.15)$$

$$R_{1i} = R_{1o} + n_hk_1(A\sin(\omega t) - x_{1i-1}) \qquad (i = n_h) \qquad (4.16)$$

$$R_{21} = R_{2o} - n_hk_2(x_{21} - x) \qquad (4.17)$$

$$R_{2i} = R_{2o} - n_hk_2(x_{2i} - x_{2i-1}) \qquad (i = 2,3,..,n_h - 1) \qquad (4.18)$$

$$R_{2i} = R_{2o} - n_hk_2(A\sin(\omega t) - x_{2i-1}) \qquad (i = n_h - 1) \qquad (4.19)$$

where P_o is the total initial tension in the vertical springs (corresponding to $x = 0$) and R_{1o}, R_{2o} are the initial tensions in the left and right horizontal

spring, respectively (corresponding to zero displacements of mass m and of the forcing arms). Finally we have

$$T(t) = 2\,K_1\,\theta(t) \tag{4.20}$$

$$\theta = \sin^{-1}(x/\ell)\ . \tag{4.21}$$

We consider, as an example, the particular case $k_1 = k_2$, $m_{h1} = m_{h2}$, $R_{1o} = R_{2o}$ (to which there correspond antisymmetric motions of the two horizontal springs) and $n_v = 4$, $n_h = 4$. Denoting $x = z_1$, $x_1 = z_3$, $x_2 = z_5$, $x_3 = z_7$, $y_1 = z_9$, and assuming that the dissipative force $g = c\,x'$ while the other dissipative forces are zero (i.e., assuming that the dissipation is entirely concentrated in the term $c\,x'$), the equations of motion can be written as

$$z_1' = z_2 \tag{4.22}$$

$$z_2' = \frac{1}{m + m_{h1}/4 + (m_1 + m_2 + m_v/4)\,z_1^2/(\ell^2 - z_1^2)}$$

$$\Big\{ - cz_2 - \frac{(m_1 + m_2 + m_v/4)\,\ell^2\,z_2^2\,z_1}{(\ell^2 - z_1^2)^2}$$

$$+ \frac{2P_o\,z_1 - 2\,(\ell + z_9)\,(4K_2)\,z_1 - 2K_1\sin^{-1}(z_1/\ell)]}{(\ell^2 - z_1^2)^{1/2}}$$

$$- 2[4k_1 - 2(4K_2)]\,z_1 + 2\,(4k_1)\,z_3\ \Big\} \tag{4.23}$$

$$z_3' = z_4 \tag{4.24}$$

$$z_4' = 4k_1\,(z_1 + z_5 - 2z_3)/(m_h/4) \tag{4.25}$$

$$z_5' = z_6 \tag{4.26}$$

$$z_6' = 4k_1\,(z_3 + z_7 - 2z_5)/(m_h/4) \tag{4.27}$$

$$z_7' = z_8 \tag{4.28}$$

$$z_8' = 4k_1\,[z_5 + A\sin(\omega t) - 2z_7]/(m_h/4) \tag{4.29}$$

$$z_9' = z_{10} \tag{4.30}$$

$$z_{10}' = -\,4K_2\{[\ell - (\ell^2 - z_1^2)^{1/2}] + 2\,z_9\}/(m_v/4)\ . \tag{4.31}$$

4.3.2 Single Degree of Freedom System

If instead of $n_v = n_h = 4$ we have $n_v = n_h = 1$, then

$$x'' + \frac{1}{m + m_{h1}/2 + (m_1 + m_2 + m_v/2)x^2/(\ell^2 - x^2)} \left\{ cx' + \frac{(m_1 + m_2 + m_v/2)\, \ell^2\, xx'^2}{(\ell^2 - x^2)^2} - 2\, \frac{(P_o - 2\ell K_2)x - K_1 \sin^{-1}(x/\ell)}{(\ell^2 - x^2)^{1/2}} + 2(k_1 - 2K_2)\, x - 2k_1 A \sin(\omega t) \right\} = 0 \, . \qquad (4.32)$$

Equation 4.32 was verified by deriving it independently from the Lagrangian of the system. The potential from which the restoring force of eq (4.32) is derived is represented as a function of the absolute value of the displacement x in figure 4.4. This double-well potential is similar to that characterizing the Duffing equation [17, p. 82]. It may therefore be expected that to eq (4.32) there can correspond forced motions similar qualitatively to those typical of the Duffing equation with forcing [17, p. 84], that is (1) periodic motions around one of the stable fixed points of the unforced Hamiltonian counterpart of the system, as shown (to within effects of noise) in figure 3.10, (2) periodic motions around the unstable fixed point, as in figure 3.8 (periodic snap-through motions), and (3) motions that are neither periodic nor quasiperiodic (chaotic motions), characterized by successions of irregular oscillations around the three fixed points, as in figure 3.1.

We note that the potential function corresponding to the multidegree of freedom system cannot be conveniently plotted, owing to its dependence upon a large number of generalized coordinates.

4.3.3 Duffing Equation

If in eq (4.32) the masses m_1, m_2, and m_v are zero, then

$$x'' + \frac{c}{M} x' - 2\, \frac{(P_o - 2K_2\ell)\, x - K_1 \sin^{-1}(x/\ell)}{M(\ell^2 - x^2)^{1/2}} + 2\, \frac{k_1 - 2K_2}{M} x = \frac{2k_1}{M} A \sin(\omega t) \qquad (4.33)$$

where $M = m + m_{h1}/2$. If, as has been done for the classical Stoker column [10, p. 54], eq (4.33) is expanded in a Taylor series and terms of order five and higher are neglected, we obtain

$$x'' + \frac{c}{M} x' + \frac{1}{M}\left(2k_1 + 2\frac{K_1}{\ell^2} - 2\frac{P_o}{\ell}\right) x + \frac{1}{M}\left(\frac{4K_1}{3\ell^4} + 2\frac{K_2}{\ell^2} - \frac{P_o}{\ell^3}\right) x^3 = \frac{2k_1}{M} A \sin(\omega t) \quad . \qquad (4.34)$$

In eq (4.34) we denote the coefficient of x' by r, the coefficient of x by $-\alpha$, the coefficient of x^3 by β, and the coefficient of $\sin(\omega t)$ by F_o. The parameters k_1, K_1, K_2, P_o, and ℓ are chosen so that $\alpha > 0$ and $\beta > 0$. By nondimensionalizing eq (4.34) so that $x = x_o w$, $t = t_o \tau$, where t_o and x_o satisfy the relations $\alpha t_o^2 = 1/2$, $\beta x_o^2 t_o^2 = 1/2$, and by using the notations $r t_o = \gamma$, $F_o t_o^2 / x_o = f$, and $\omega t_o = \Omega$, we obtain the standard form of the Duffing equation

$$w'' + \gamma w' - \frac{1}{2} w + \frac{1}{2} w^3 = f \sin(\Omega \tau) \quad . \qquad (4.35)$$

Useful explorations of the motions corresponding to various regions of the parameter space for the Duffing equation are reported in [11]. For this reason the Duffing equation was used as a guide in preliminary attempts to obtain chaotic motions of the one-degree of freedom system represented by eq (4.32). We note, however, that unlike eq (4.32), eq (4.35) cannot be viewed as an approximation to the experimental device since masses m_1, m_2, and m_v are negligibly small.

5. NUMERICAL SIMULATIONS

Numerical simulations were performed for two purposes. First, an attempt was made to reproduce by numerical simulation the chaotic motion obtained experimentally. Second, for a given set of system parameters, simulations were performed with a view to ascertaining whether two models, one representing a simplified version of the other, yielded motions that belonged to the same of the three types of response listed at the end of section 4.3.2. Motions belonging to the same type of response will be referred to here as qualitatively similar.

5.1 Numerical Simulation of Observed Chaotic Motion

It was suggested in section 4.1 that the mass of the springs appears to be a significant modeling factor. For this reason we modeled the motion of the experimental device by dividing the vertical and each of the horizontal springs into several segments having the respective masses lumped at their centers. We used eqs (4.22) through (4.31), which correspond to the division of each of the tension springs into four segments, and in which the dissipative force was asssumed to be proportional to x', the factor of proportionality being a constant c. The torsional stiffness was modeled by eq (2.1), and the various parameters of the system had the values given in sections 2 and 3. Although we did not attempt to perform exhaustive numerical studies, we ascertained that chaotic motions were obtained for a fairly broad range of values c. For $c = 3.0$,

[3] J. M. T. Thompson and H. B. Stewart, Nonlinear Dynamics and Chaos, John Wiley and Sons, New York, 1986.

[4] E. Simiu and G. R. Cook, "Periodic, Quasiperiodic and Chaotic Motions of Forced and Autonomous Galloping Oscillators," Proceedings of the 8th Colloquium on Industrial Aerodynamics, Department of Aeronautics, Fachhochschule Aachen, Aachen, W. Germany, Sep. 4-7, 1989, Part 1, pp. 167-178.

[5] D. J. Olinger and K. R. Sreenivasan, "Nonlinear Dynamics of the Wake of an Oscillating Cylinder," Physical Review Letters, Vol. 60, No. 9, pp. 2798-2801, 1988.

[6] R. H. Scanlan and J. J. Tomko, "Airfoil and Bridge Deck Flutter Derivatives," Journal of the Engineering Mechanics Division, ASCE, Vol. 97, pp. 1717-1737, 1971.

[7] S. Wiggins, Global Bifurcations and Chaos, Springer-Verlag, New York, 1988.

[8] F. C. Moon and P. J. Holmes, "A Magnetoelastic Strange Attractor," Journal of Sound and Vibration, Vol. 69, No. 2, pp. 285-296, 1979.

[9] H. Clemens and J. Wauer, "Durchschlagen vorgekruemmter Staebe unter harmonisch pulsierender Belastung,", Proceedings of the 8th International Conference on Nonlinear Oscillations, Institute of Thermomechanics, Czechoslovak Academy of Sciences, Prague, 1978, pp. 191-197.

[10] J. J. Stoker, Nonlinear Vibrations, Interscience Publishers Inc, New York, 1950.

[11] E. H. Dowell and C. Pezeshki, "On the Understanding of Chaos in Duffing's Equation Including a Comparison with Experiment," Journal of Applied Mechanics, ASME, Vol. 53, March 1986, pp. 5-9.

[12] J. M. T. Thompson, Instabilities and Catastrophes in Science and Engineering, John Wiley and Sons, New York, 1982.

[13] P. Berge, Y. Pomeau, and C. Vidal, Order within Chaos, John Wiley and Sons, New York, 1984.

[14] F. C. Moon, Chaotic Vibrations, John Wiley and Sons, New York, 1987.

[15] F. Sullivan and F. Hunt, "How to Estimate Capacity Dimension," Nuclear Physics B, (Proc. Suppl.), Vol. 5B, 1988, pp. 125-128.

[16] A. Wolf, J. B. Swift, H. L. Swinney, and J. A. Vastano, "Determining Lyapunov Exponents from a Time Series," Physica D, 1985, pp. 285-317.

[17] J. Guckenheimer and P. Holmes, Nonlinear Oscillations, Dynamical Systems, and Bifurcations of Vector Fields, Springer-Verlag, New York, 1983.

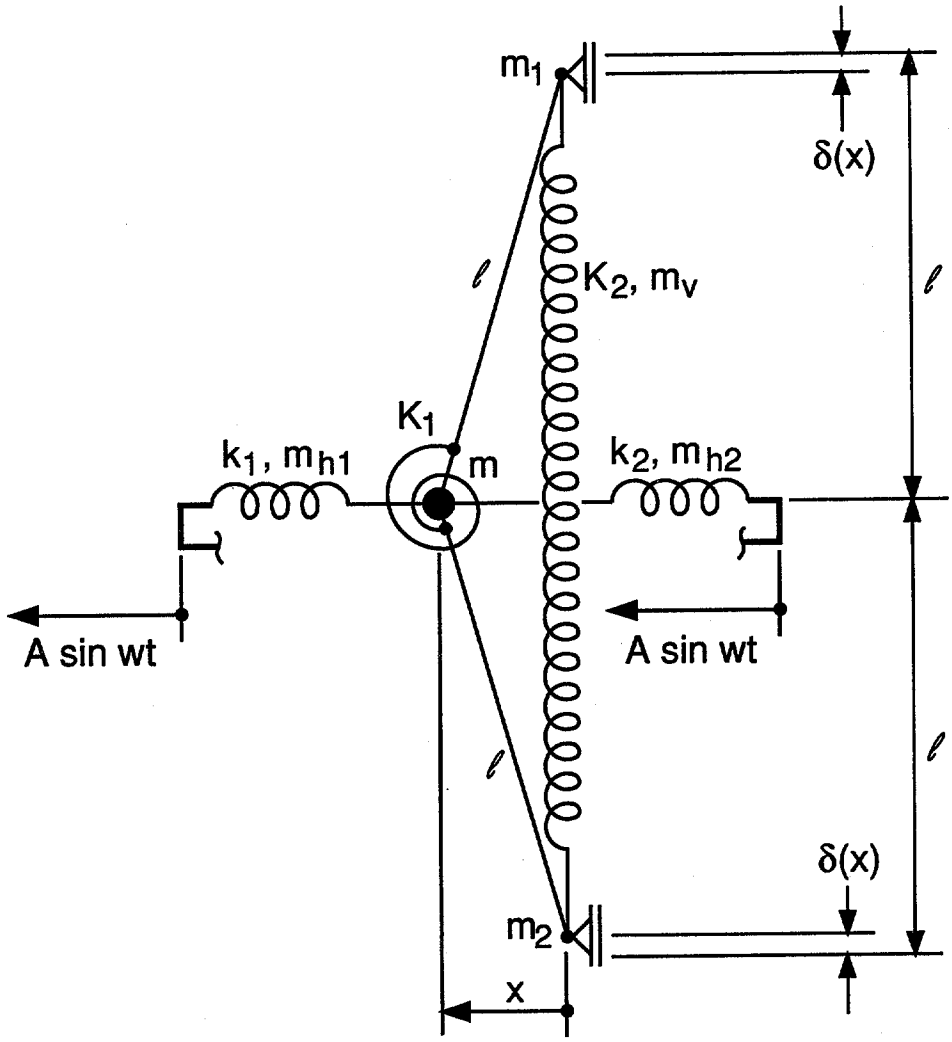

Fig. 2.1 Schematic of Forced Modified Stoker Column.

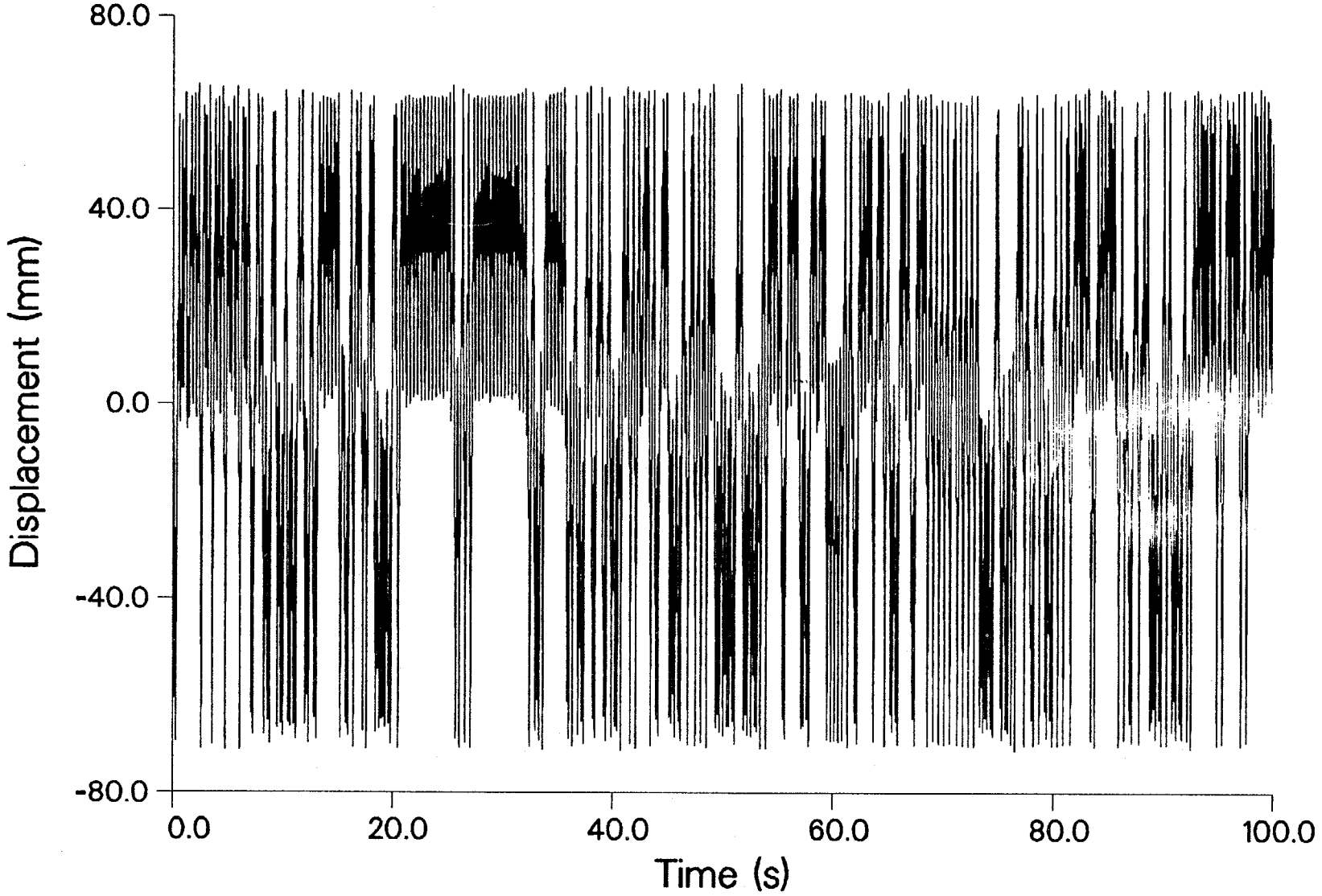

Fig. 3.1a Time History of Displacement x.

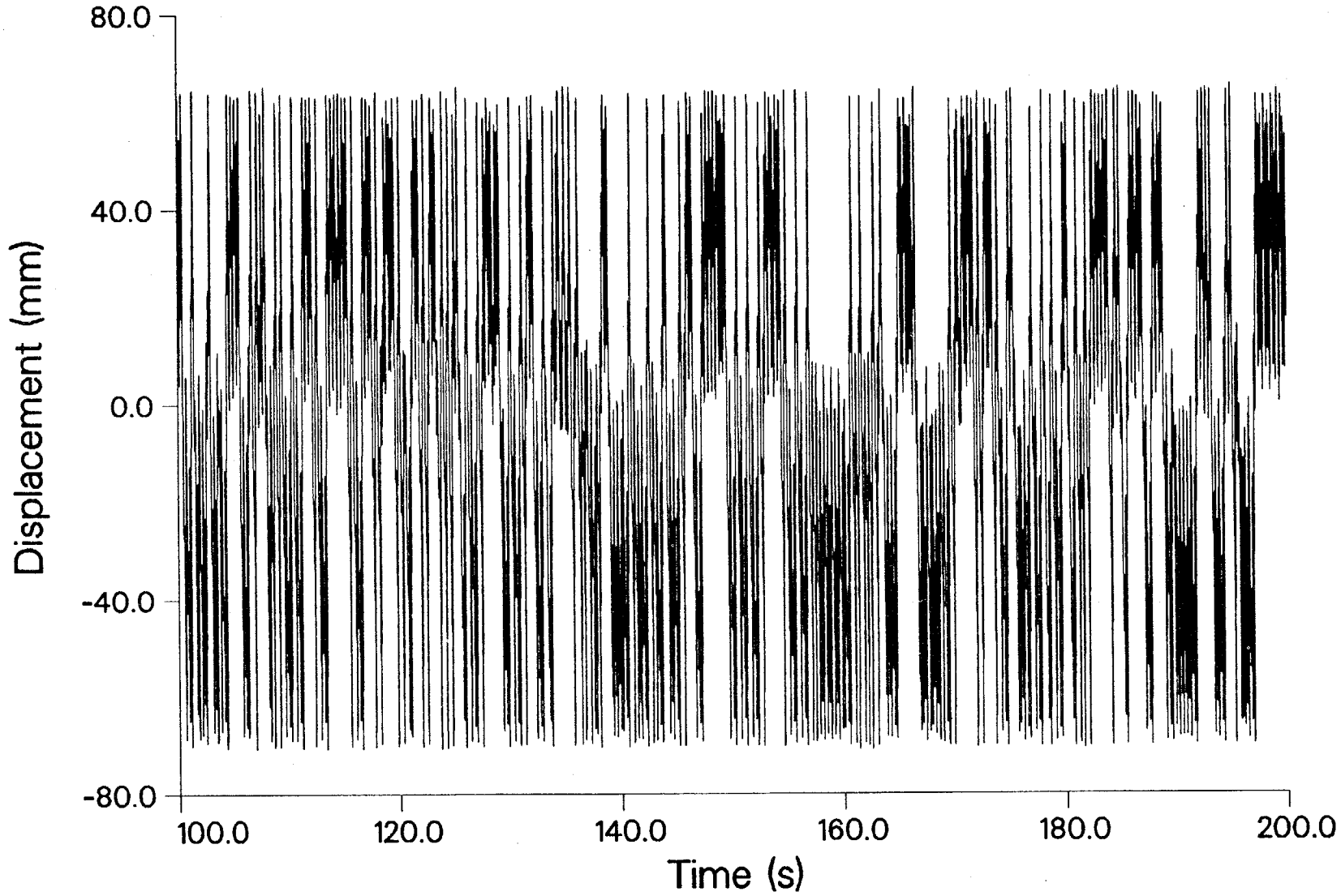

Fig. 3.1b Time History of Displacement x.

which would correspond in a linear system with unit mass and stiffness $2k_1$ to a damping ratio of about 7%, we obtained the time history of figure 5.1. While the motions of figures 3.2 and 5.1 are similar qualitatively, they are clearly different quantitatively. We note that quantitative differences between experimental and numerically simulated motions were also pointed out for a similar oscillator in [17, p. 84]. Changing the constant c, or assuming that c was constant for $|x| < 0.066$ and increased linearly for $|x| > 0.066$ until it reached at $|x| = 0.075$ a value n times larger than for small $|x|$ ($n = 2, 3, \ldots, 10$), did not result in a substantially improved reproduction of the experimental motion. The stroboscopic Poincare plot and the spectral density function corresponding to figure 5.1 are shown in figures 5.2 and 5.3, respectively. Note that the maximum velocities are considerably higher for the simulated than for the observed motion (fig. 5.2 versus fig. 3.4).

Detailed modeling and measurements of the dissipative forces and of the spring stiffnesses under dynamic conditions -- particularly for the torsional springs -- were beyond the scope of this project. Had such modeling and measurements been performed, and had the springs been divided for simulation purposes into more that four segments, it is likely that the observed chaotic motion would have been reproduced more closely. Nevertheless, we note that in spite of the imperfect modeling of the dissipative forces and possibly of spring stiffnesses as well, the modeling of the device by a system with 10 degrees of freedom (reduced owing to symmetries and antisymmetries to a system with 5 degrees of freedom) was capable of reproducing qualitatively the observed chaotic motion.

5.2 Effect of Simplified Representation of the Device as a One Degree of Freedom System

We also attempted to reproduce qualitatively the observed chaotic motion by modeling the device as a system with three masses. As shown in section 4, owing to the geometrical constraints of the device, if the spring masses are neglected, the system with masses m, m_1 and m_2 (to which tributary spring masses are added) has one degree of freedom. We therefore simulated the motion of the device by using eq (4.32), with the same dissipative forces and stiffnesses as in the simulations of the corresponding multidegree of freedom system (sec. 5.1). In none of the tens of cases for which chaotic motion was obtained for the multidegree of freedom system did the corresponding one degree of freedom system result in chaotic motion. Additional tens of simulations for the one degree of freedom system, in which the parameters defining the assumed dissipative forces were varied from simulation to simulation while all other parameters were kept equal to their counterparts in the experimental device, also failed in all cases to yield chaotic motion.

It may be that, had we used a model that reproduced more closely the actual dissipative forces (and possibly also the dynamic spring forces), chaotic motion could have been obtained even by modeling the device as a one degree of freedom system. Nevertheless, our results allow us to draw the interesting conclusion that motions of the multidegree of freedom systems represented by the simulations of section 5.1 cannot be reproduced even qualitatively if those systems are modeled as one degree of freedom systems. This result differs from that obtained for the oscillator discussed in [17, p. 84], for which the approximation of a continuous beam by a one degree of freedom mass did not alter

the observed behavior qualitatively. The effect of the additional degrees of freedom of the system is significant in our case owing to the relative magnitudes of relevant parameters, in particular the spring masses and stiffnesses, masses m, m_1 and m_2, and the forcing frequency ω.

6. SUMMARY AND CONCLUSIONS

Following a description of the modified Stoker column as constructed at the Center for Building Technology, National Institute of Standards and Technology, we presented records of typical motions of that device as measured in the laboratory, including periodic motion around a stable fixed point, periodic snap-through motion, and chaotic motion. Characterizations of the recorded chaotic motion included: the autocorrelation function, which decays and then vanishes (to within noise effects) after a 0.74 s lag, thus indicating that knowledge of past history of the motion cannot be used to make deterministic inferences on future behavior; the spectral density plot, which exhibits relatively substantial broadband components, as is expected for a time history with decaying autocorrelation; the capacity dimensions of a Poincare plot of the strange attractor of the motion (N = 1.25) and of the attractor constructed by embedding the time history in a three-dimensional phase space (N = 2.3); and the Lyapounov exponent, whose estimated value was approximately 3.00.

The stiffness measurements for the springs used in the construction of the device were performed under static conditions, and no measurements were performed of the dissipative forces occurring during the motion. Nevertheless, numerical simulations based on an analytical model in which the spring stiffnesses measured under static conditions were used and the damping was assumed to be viscous yielded chaotic motions qualitatively similar to those recorded in the laboratory. That model entailed the representation of the device as a multidegree of freedom system to account for the fact that, owing to the spring properties, times required for disturbances to travel from one end of a spring to the other are significant in relation to the forcing period of the system. On the other hand, we were unsuccessful in our attempts to simulate the chaotic motion when representing the device as a one degree of freedom system (i.e., by assuming that disturbances are propagated through the springs instantaneously). To our knowledge this is the first instance of an experimental structural system with continuous members for which a qualitatively successful simulation of the chaotic motion appears to require the inclusion in the model of additional degrees of freedom to account for the effects of continuity.

A videotape of the chaotic motions of the device is available upon request from the authors.

7. REFERENCES

[1] J. M. T. Thompson, "Complex Dynamics of Compliant Offshore Structures," Proceedings, Royal Society of London, A 387, pp. 407-427, 1983.

[2] J. M. T. Thompson, A. R. Bokaian, R. Ghaffari, "Subharmonic and Chaotic Motions of Compliant Offshore Structures and Articulated Mooring Towers," Journal of Energy Resources Technology, ASME, Vol. 106, pp. 191-198, June 1984.

[3] J. M. T. Thompson and H. B. Stewart, Nonlinear Dynamics and Chaos, John Wiley and Sons, New York, 1986.

[4] E. Simiu and G. R. Cook, "Periodic, Quasiperiodic and Chaotic Motions of Forced and Autonomous Galloping Oscillators," Proceedings of the 8th Colloquium on Industrial Aerodynamics, Department of Aeronautics, Fachhochschule Aachen, Aachen, W. Germany, Sep. 4-7, 1989, Part 1, pp. 167-178.

[5] D. J. Olinger and K. R. Sreenivasan, "Nonlinear Dynamics of the Wake of an Oscillating Cylinder," Physical Review Letters, Vol. 60, No. 9, pp. 2798-2801, 1988.

[6] R. H. Scanlan and J. J. Tomko, "Airfoil and Bridge Deck Flutter Derivatives," Journal of the Engineering Mechanics Division, ASCE, Vol. 97, pp. 1717-1737, 1971.

[7] S. Wiggins, Global Bifurcations and Chaos, Springer-Verlag, New York, 1988.

[8] F. C. Moon and P. J. Holmes, "A Magnetoelastic Strange Attractor," Journal of Sound and Vibration, Vol. 69, No. 2, pp. 285-296, 1979.

[9] H. Clemens and J. Wauer, "Durchschlagen vorgekruemmter Staebe unter harmonisch pulsierender Belastung,", Proceedings of the 8th International Conference on Nonlinear Oscillations, Institute of Thermomechanics, Czechoslovak Academy of Sciences, Prague, 1978, pp. 191-197.

[10] J. J. Stoker, Nonlinear Vibrations, Interscience Publishers Inc, New York, 1950.

[11] E. H. Dowell and C. Pezeshki, "On the Understanding of Chaos in Duffing's Equation Including a Comparison with Experiment," Journal of Applied Mechanics, ASME, Vol. 53, March 1986, pp. 5-9.

[12] J. M. T. Thompson, Instabilities and Catastrophes in Science and Engineering, John Wiley and Sons, New York, 1982.

[13] P. Berge, Y. Pomeau, and C. Vidal, Order within Chaos, John Wiley and Sons, New York, 1984.

[14] F. C. Moon, Chaotic Vibrations, John Wiley and Sons, New York, 1987.

[15] F. Sullivan and F. Hunt, "How to Estimate Capacity Dimension," Nuclear Physics B, (Proc. Suppl.), Vol. 5B, 1988, pp. 125-128.

[16] A. Wolf, J. B. Swift, H. L. Swinney, and J. A. Vastano, "Determining Lyapunov Exponents from a Time Series," Physica D, 1985, pp. 285-317.

[17] J. Guckenheimer and P. Holmes, Nonlinear Oscillations, Dynamical Systems, and Bifurcations of Vector Fields, Springer-Verlag, New York, 1983.

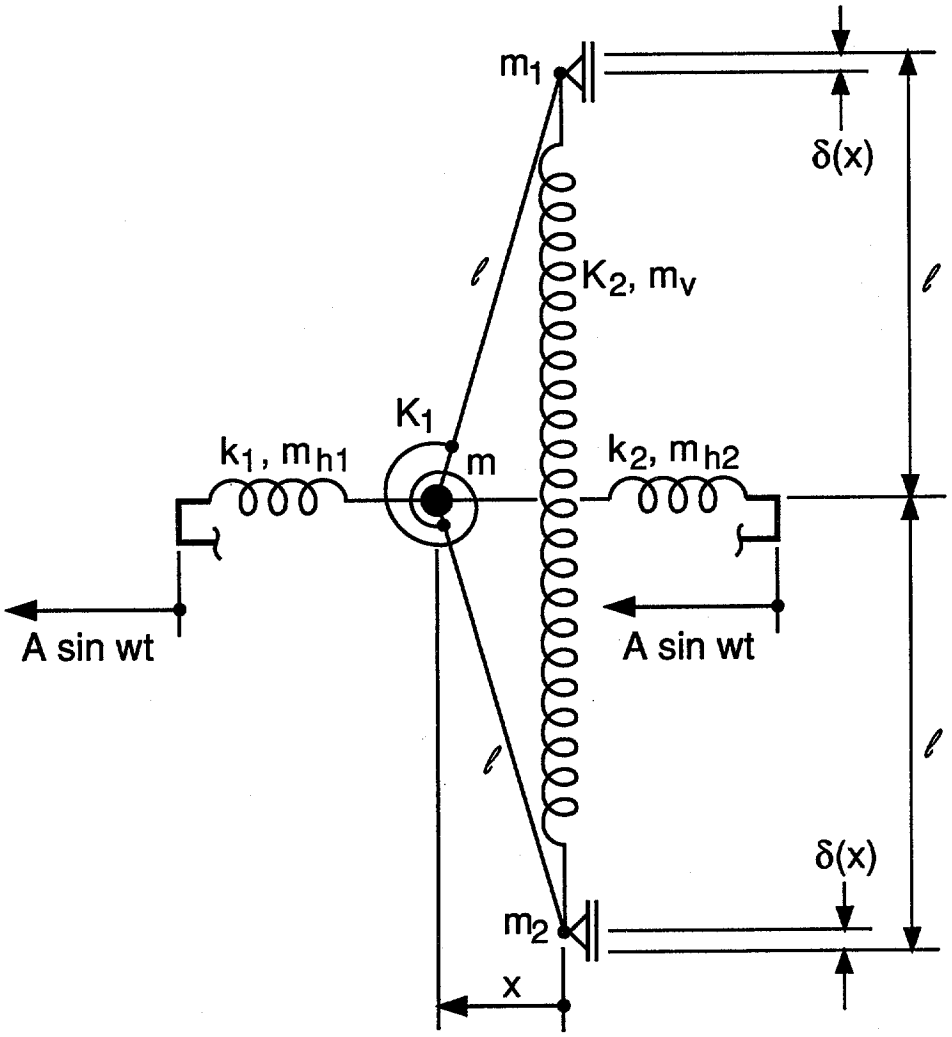

Fig. 2.1 Schematic of Forced Modified Stoker Column.

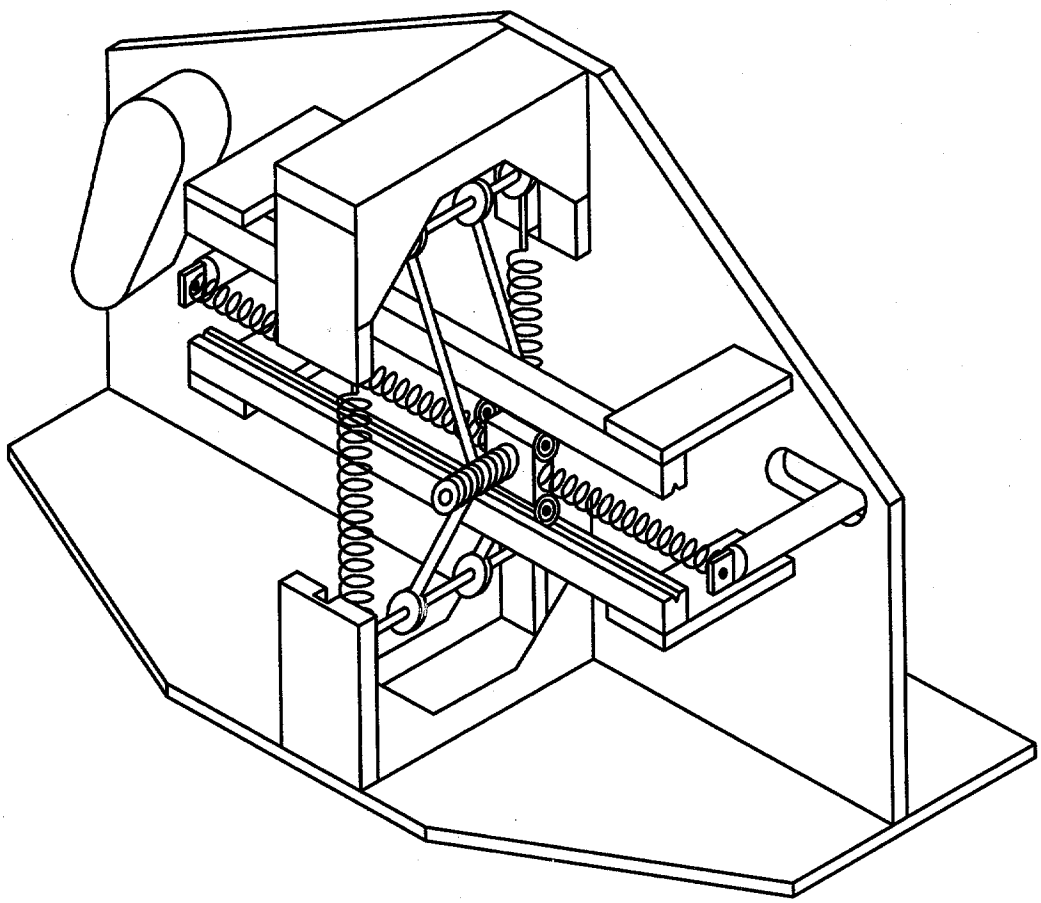

Fig. 2.2 Drawing of Forced Modified Stoker Column.

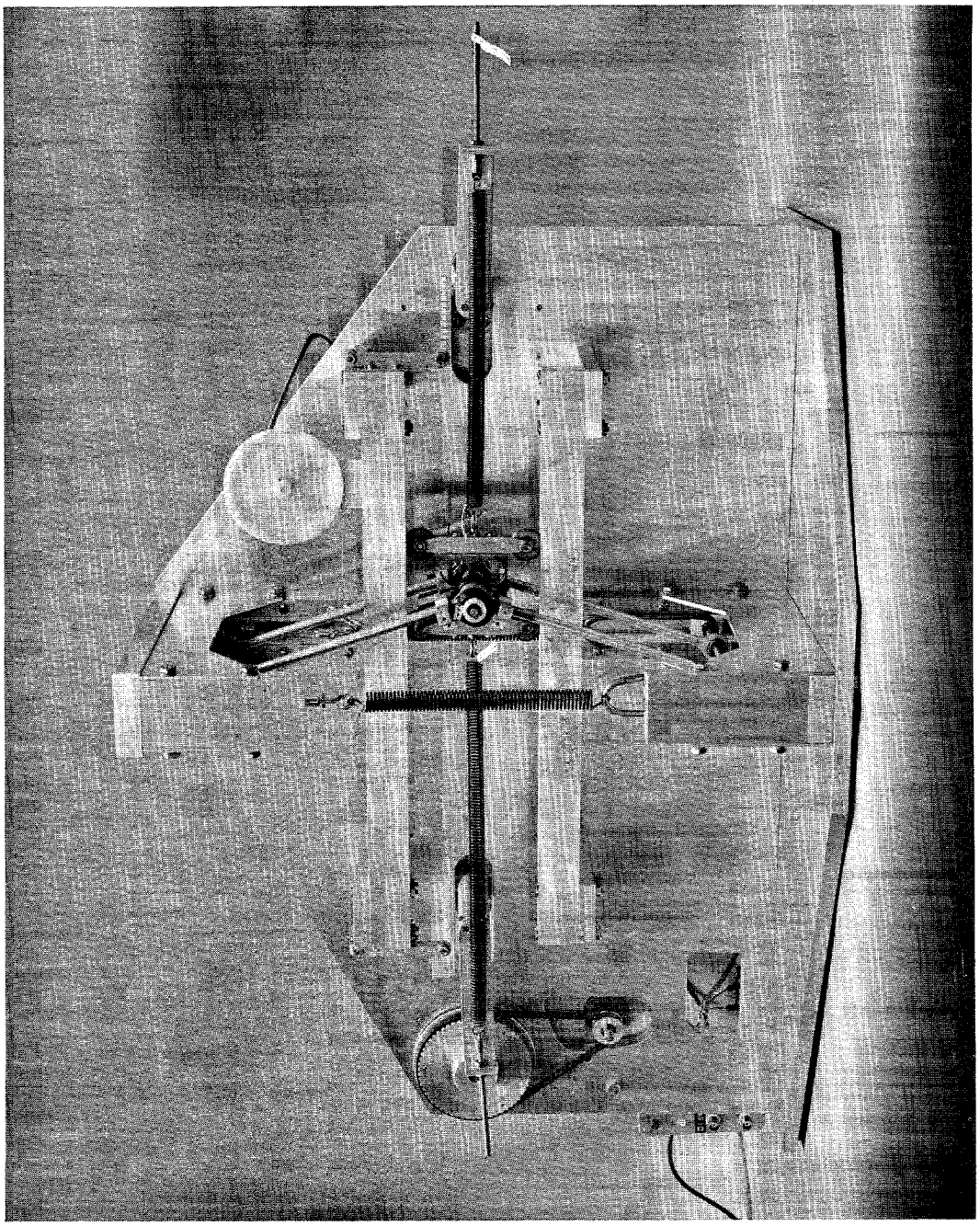

Fig. 2.3 Photograph of Forced Modified Stoker Column.

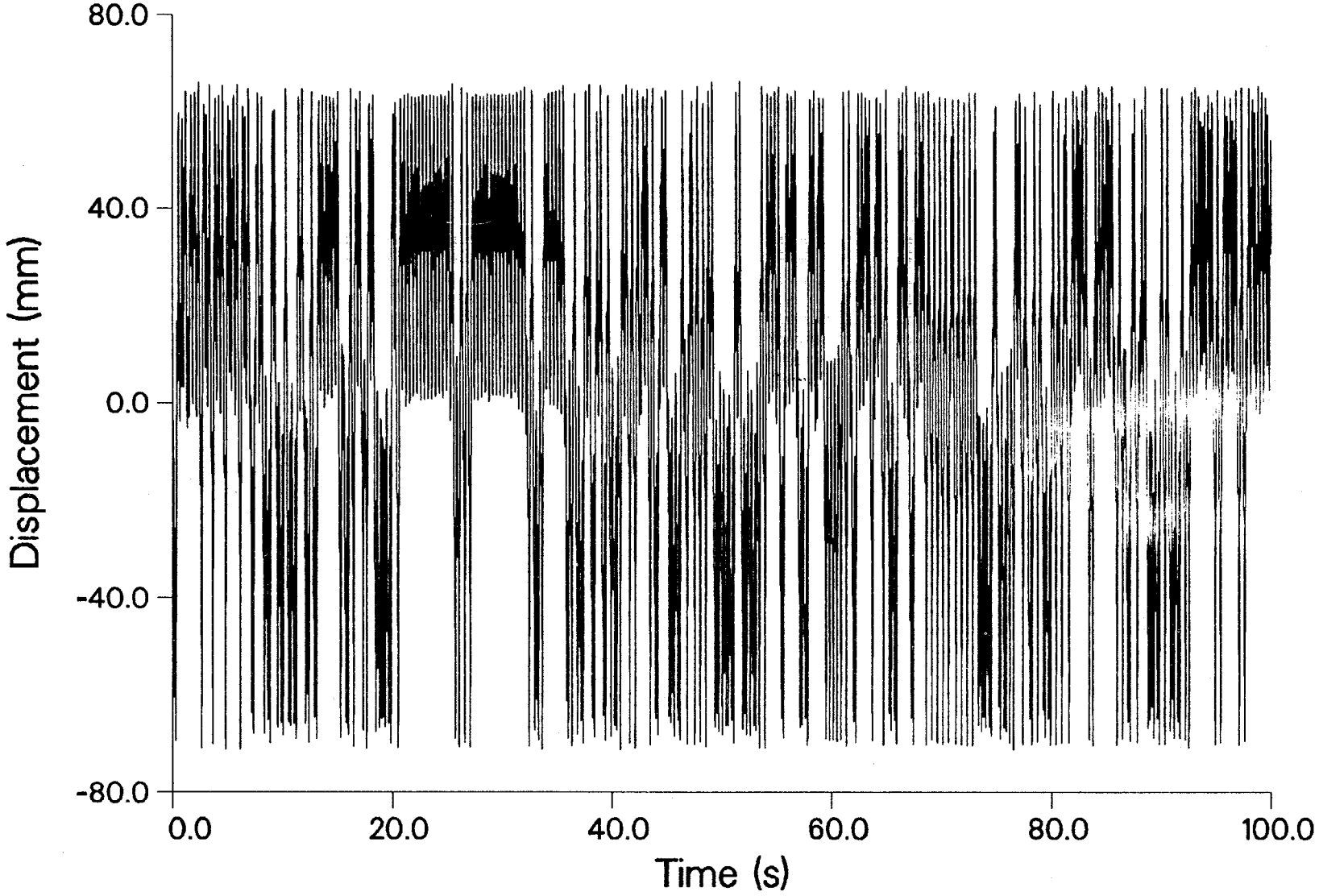

Fig. 3.1a Time History of Displacement x.

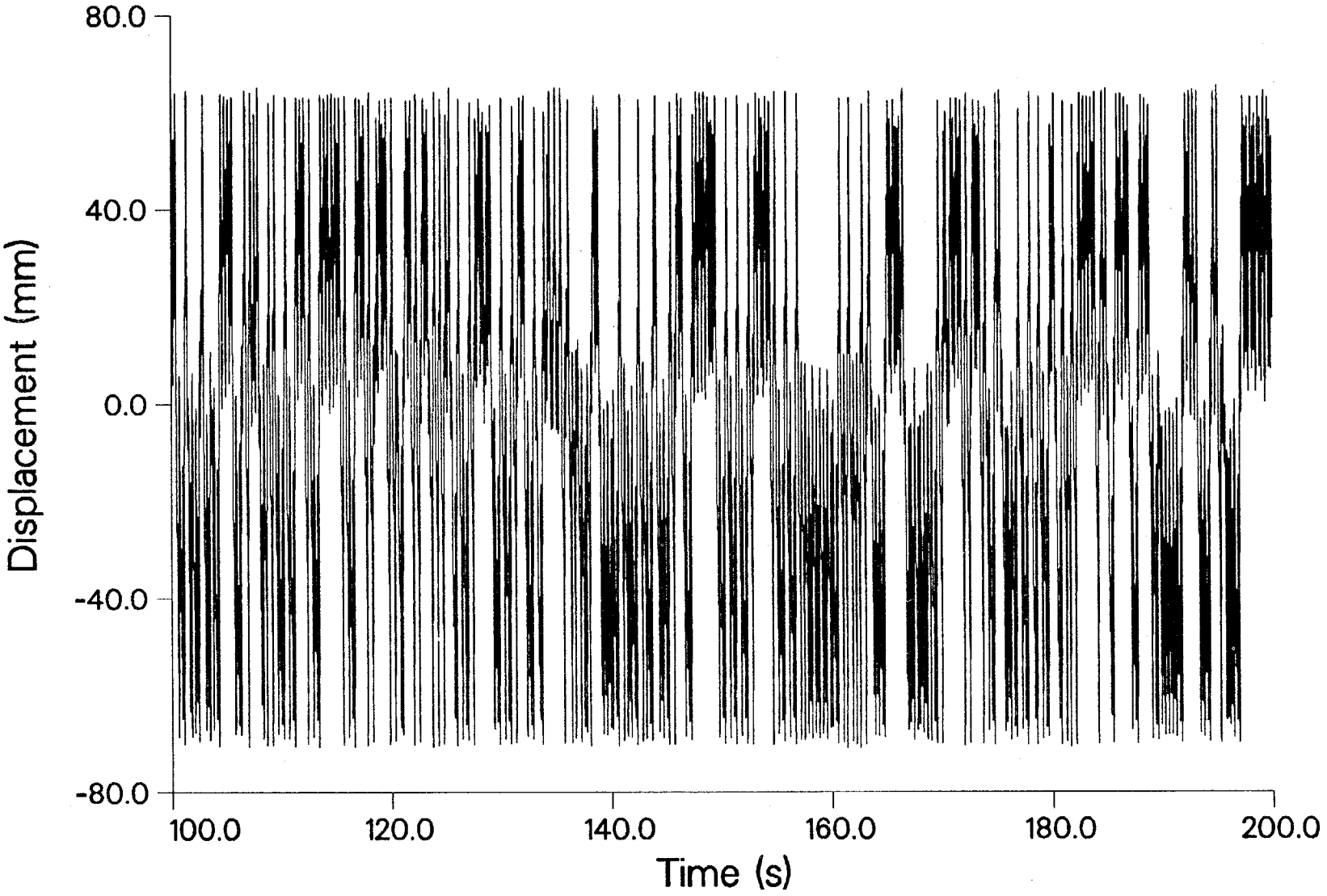

Fig. 3.1b Time History of Displacement x.

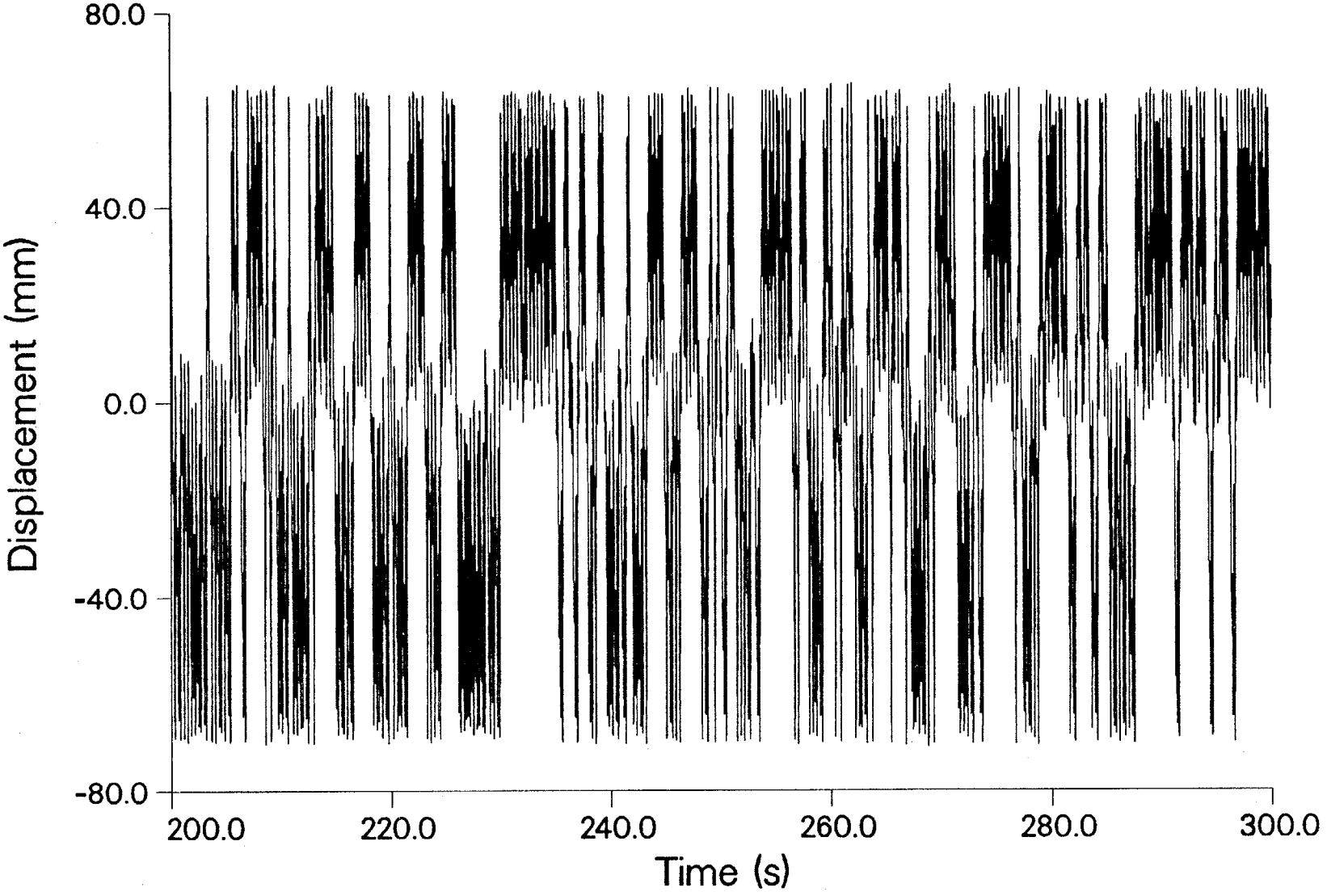

Fig. 3.1c Time History of Displacement x.

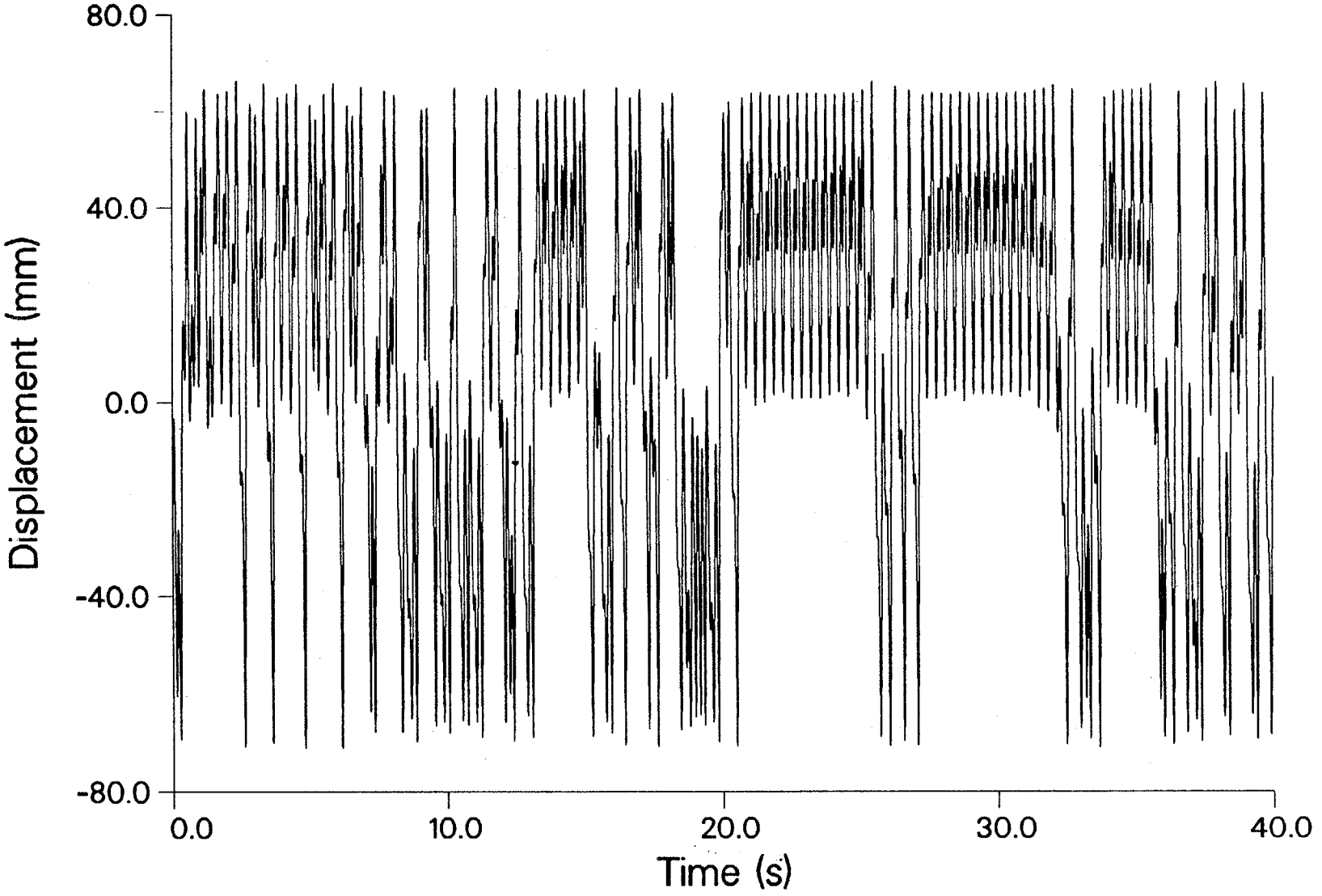

Fig. 3.2 Time History of Displacement x.

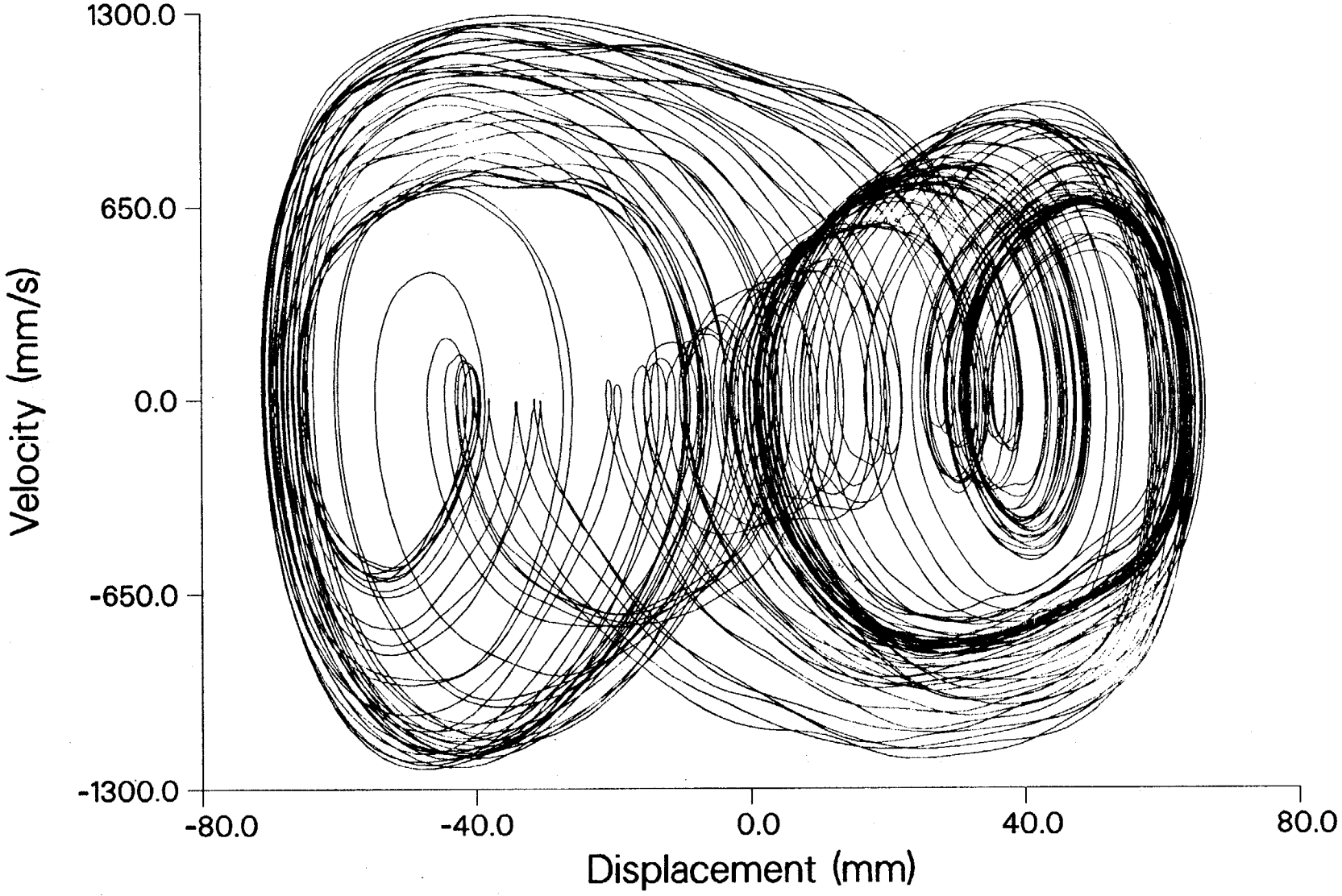

Fig. 3.3 Phase Plane Diagram.

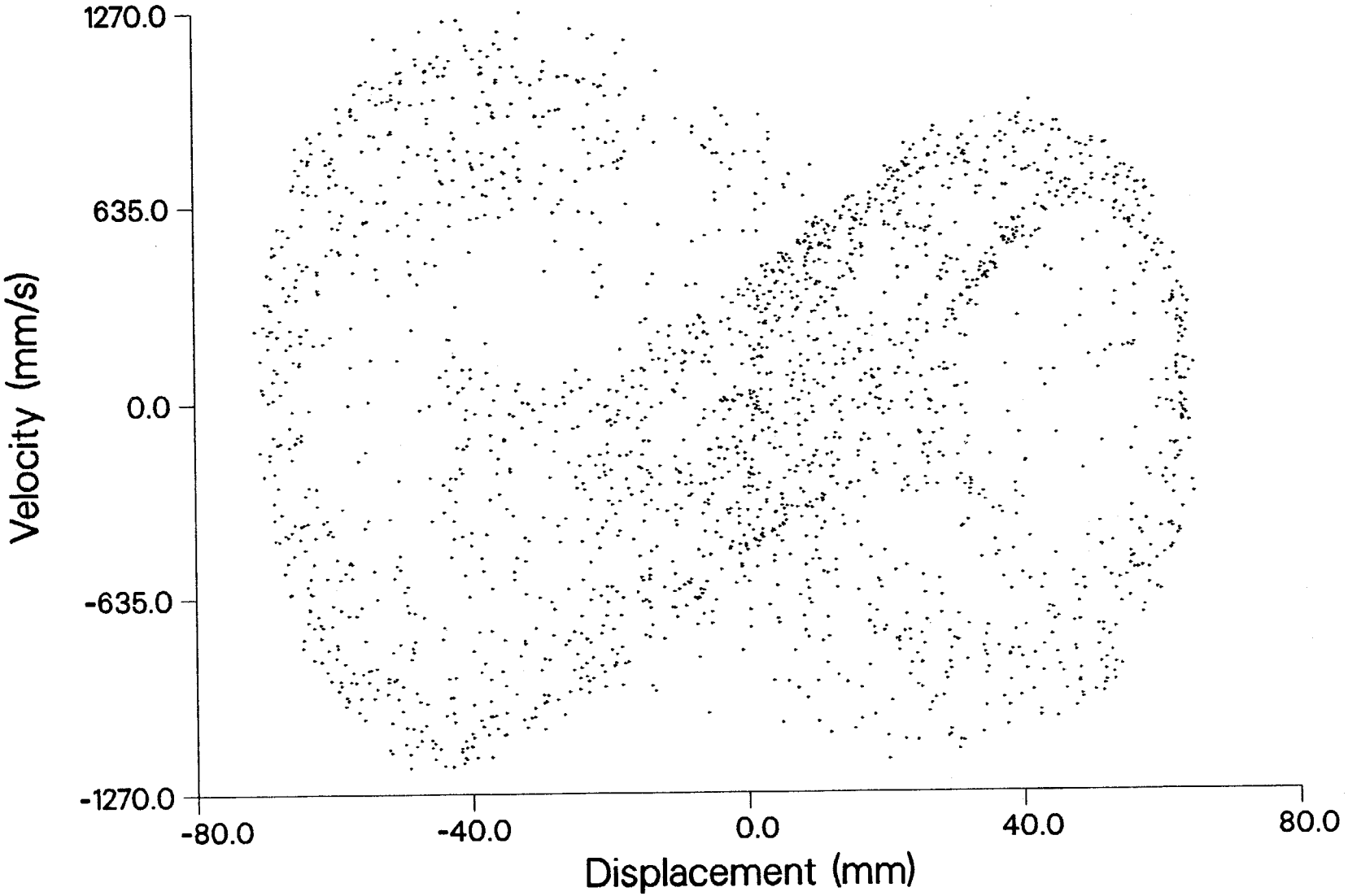

Fig. 3.4 Intersections of Orbit x, x', t with Planes $t = 2\pi n/\omega$ ($n = 1,2,\ldots$).

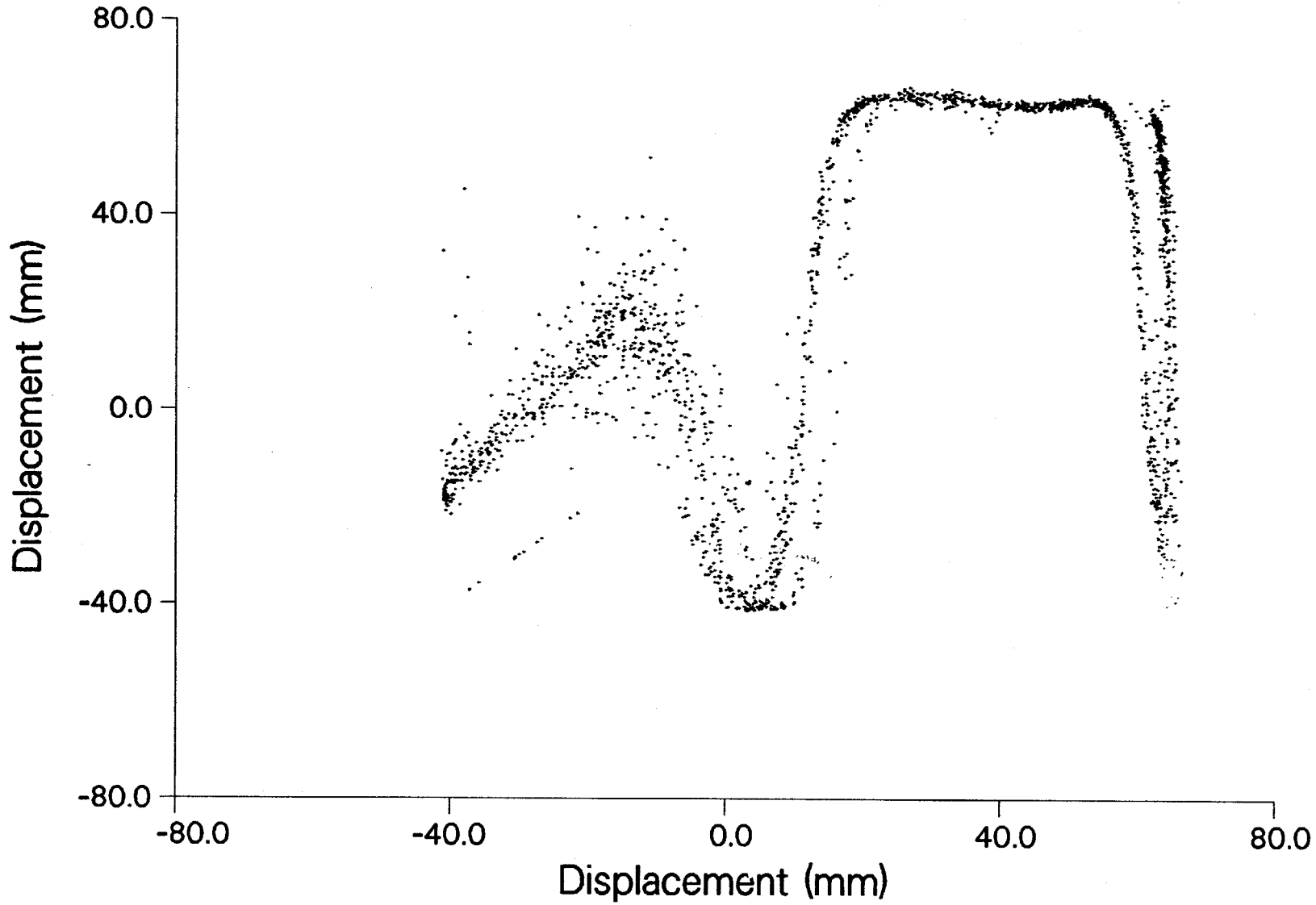

Fig. 3.5 Mapping of Successive Local Maxima of x, x_i versus x_{i+1}.

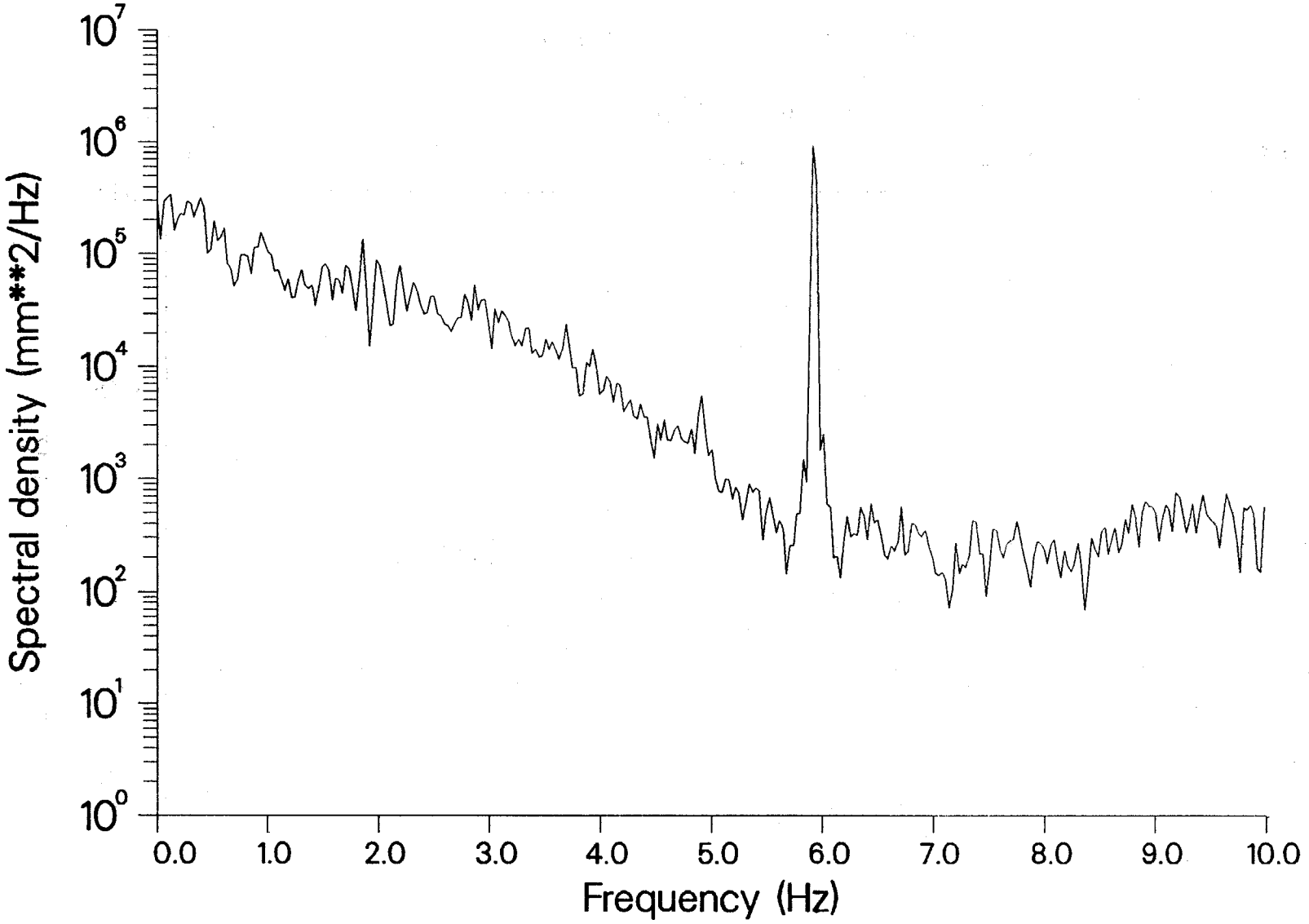

Fig. 3.6 Spectral Density Function of x.

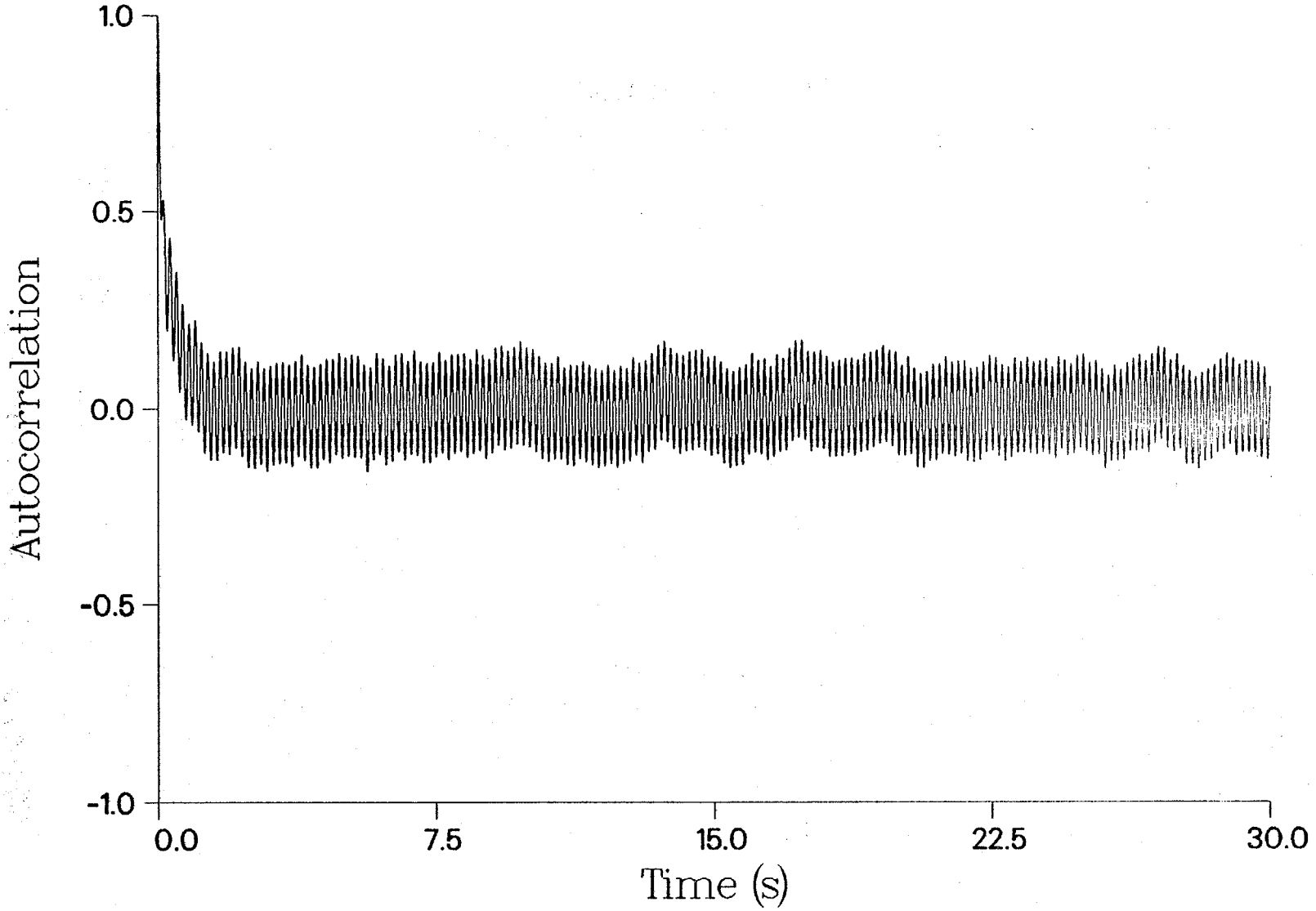

Fig. 3.7 Autocorrelation Function of x.

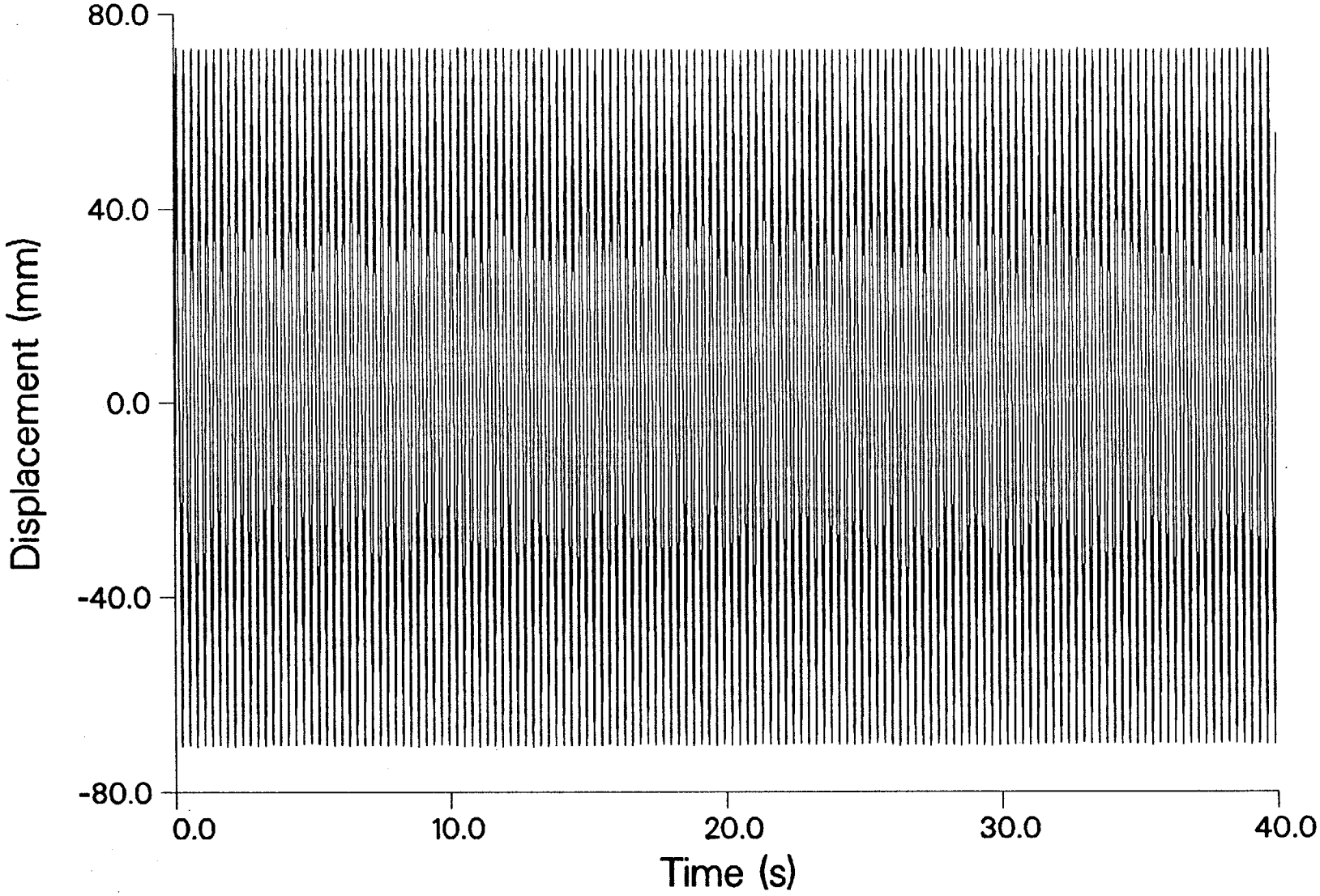

Fig. 3.8 Snap-through Oscillations.

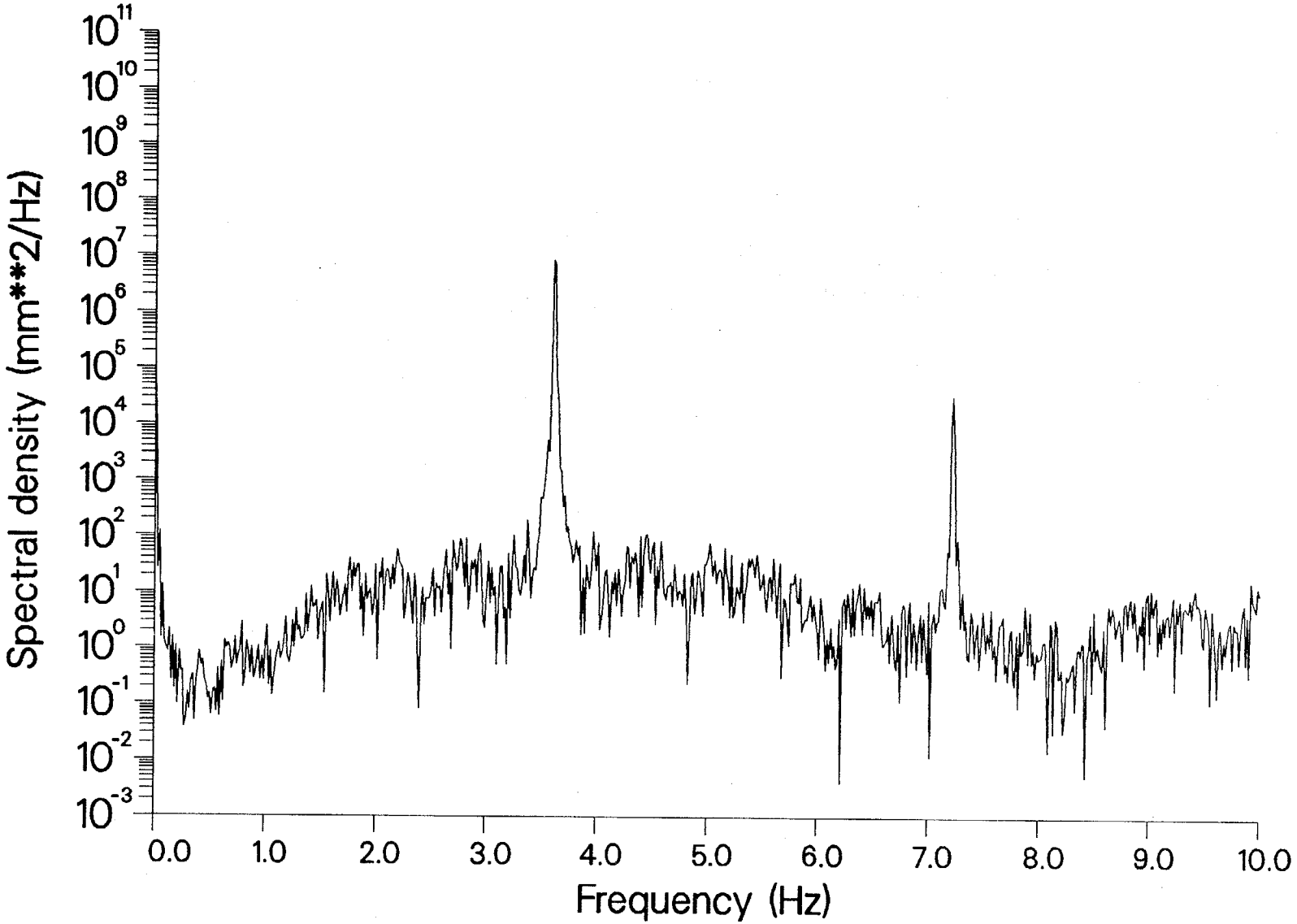

Fig. 3.9 Spectral Density of Snap-through Oscillatory Motion.

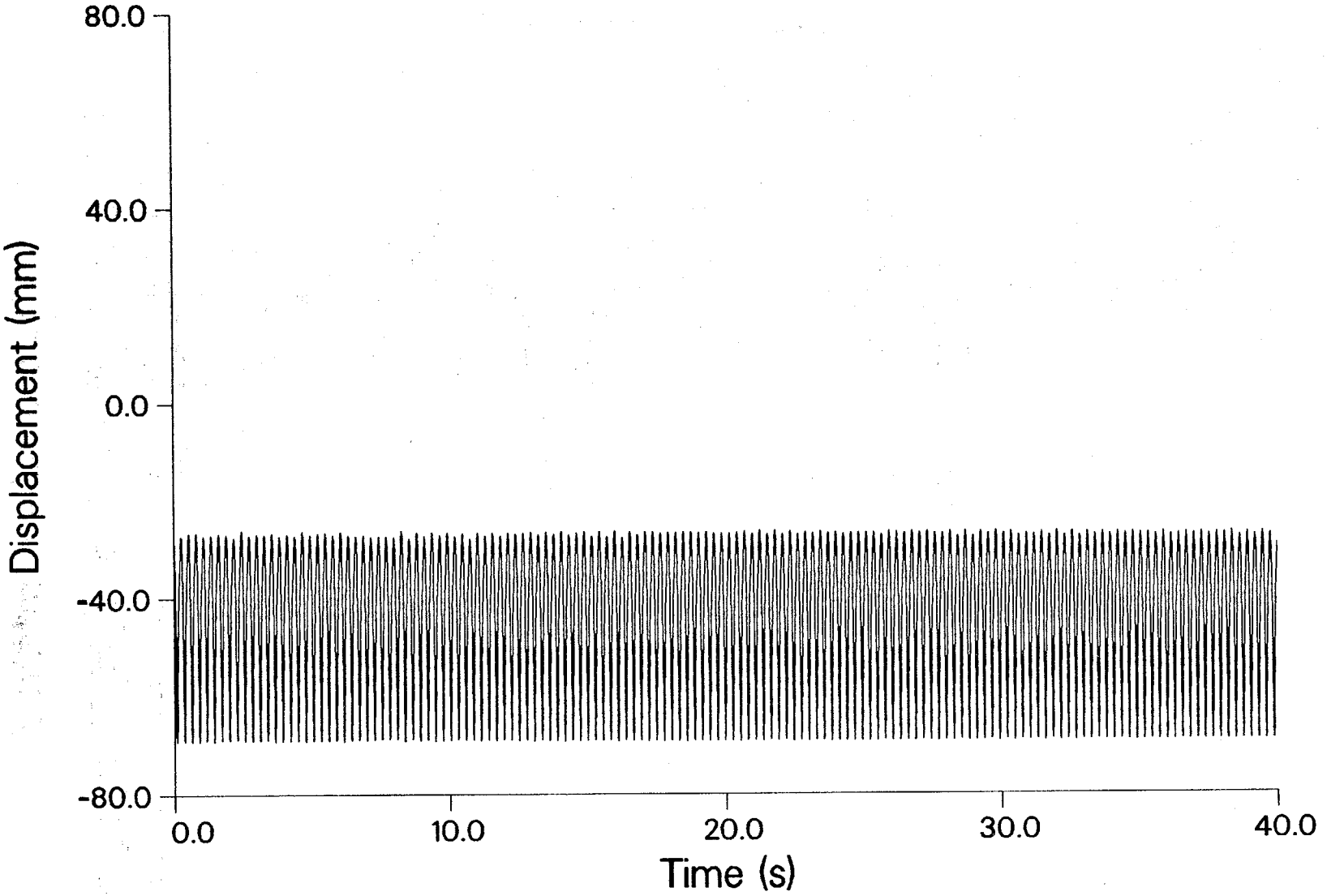

Fig. 3.10 Oscillations Around a Stable Fixed Point of the Unforced Motion.

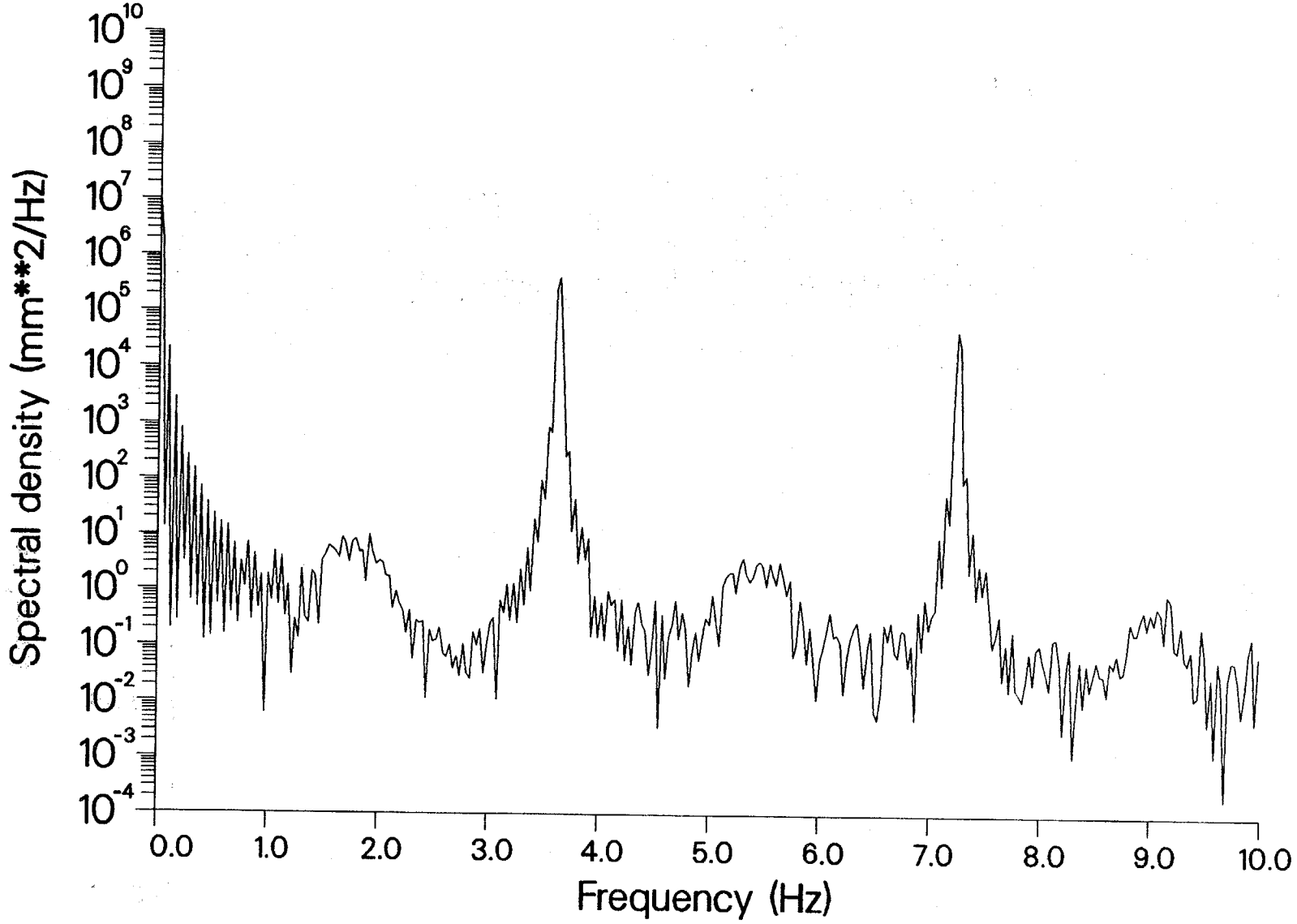

Fig. 3.11 Spectral Density of Oscillatory Motion Around Fixed Point.

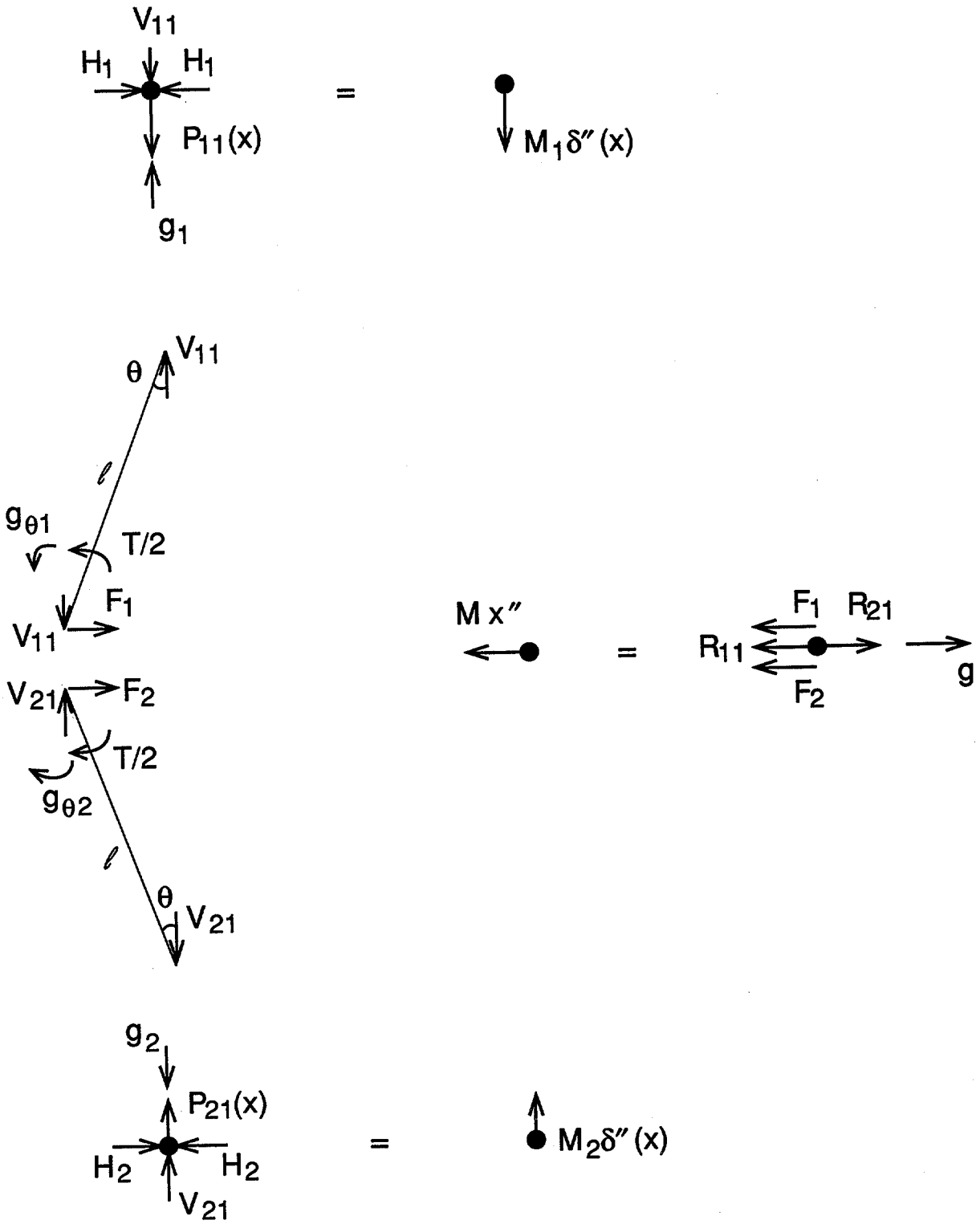

Fig. 4.1 Free Body Diagrams.

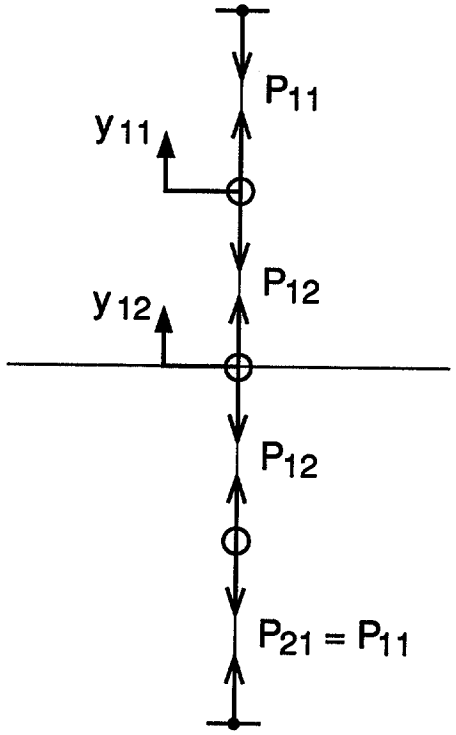

Fig. 4.2 Lumped Masses Representing Vertical Springs ($n_v = 4$).

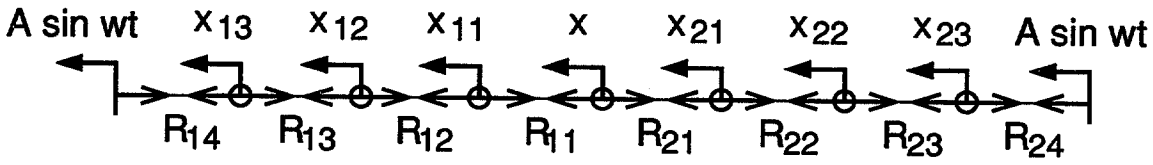

Fig. 4.3 Lumped Masses Representing Horizontal Springs ($n_h = 4$).

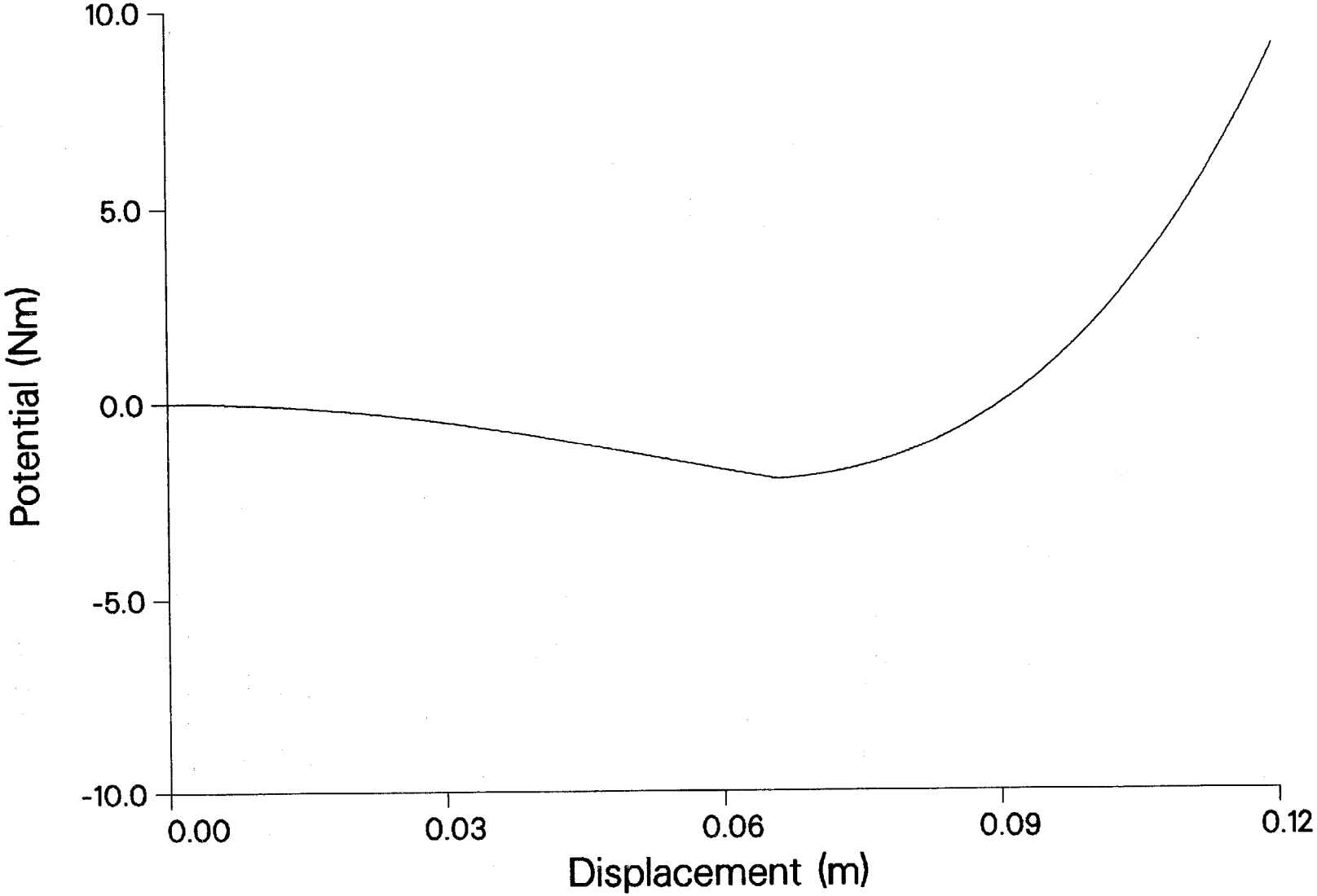

Fig. 4.4 Dependence of Potential Function on Displacement |x| for One Degree of Freedom System.

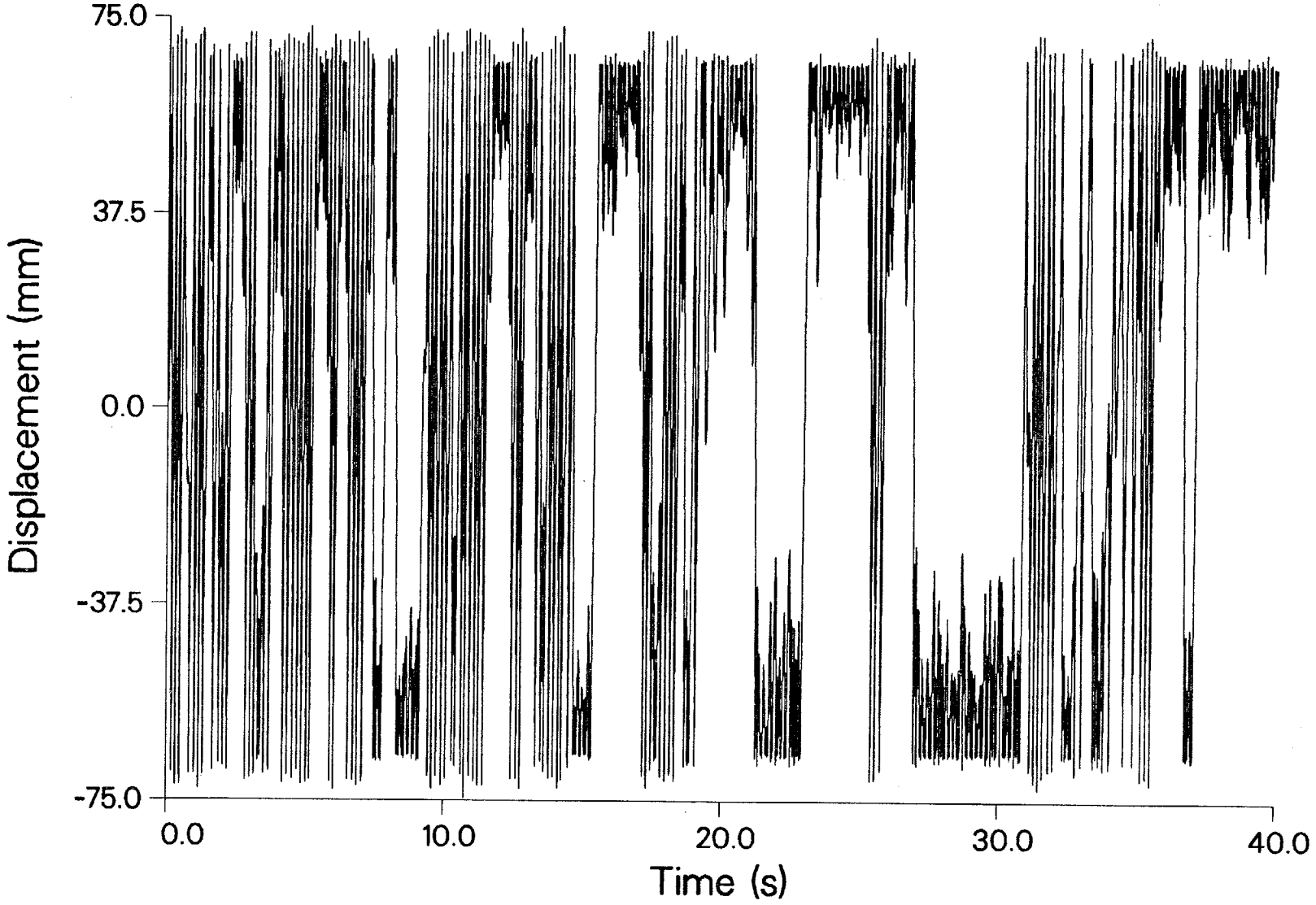

Fig. 5.1 Time History of Simulated Chaotic Motion.

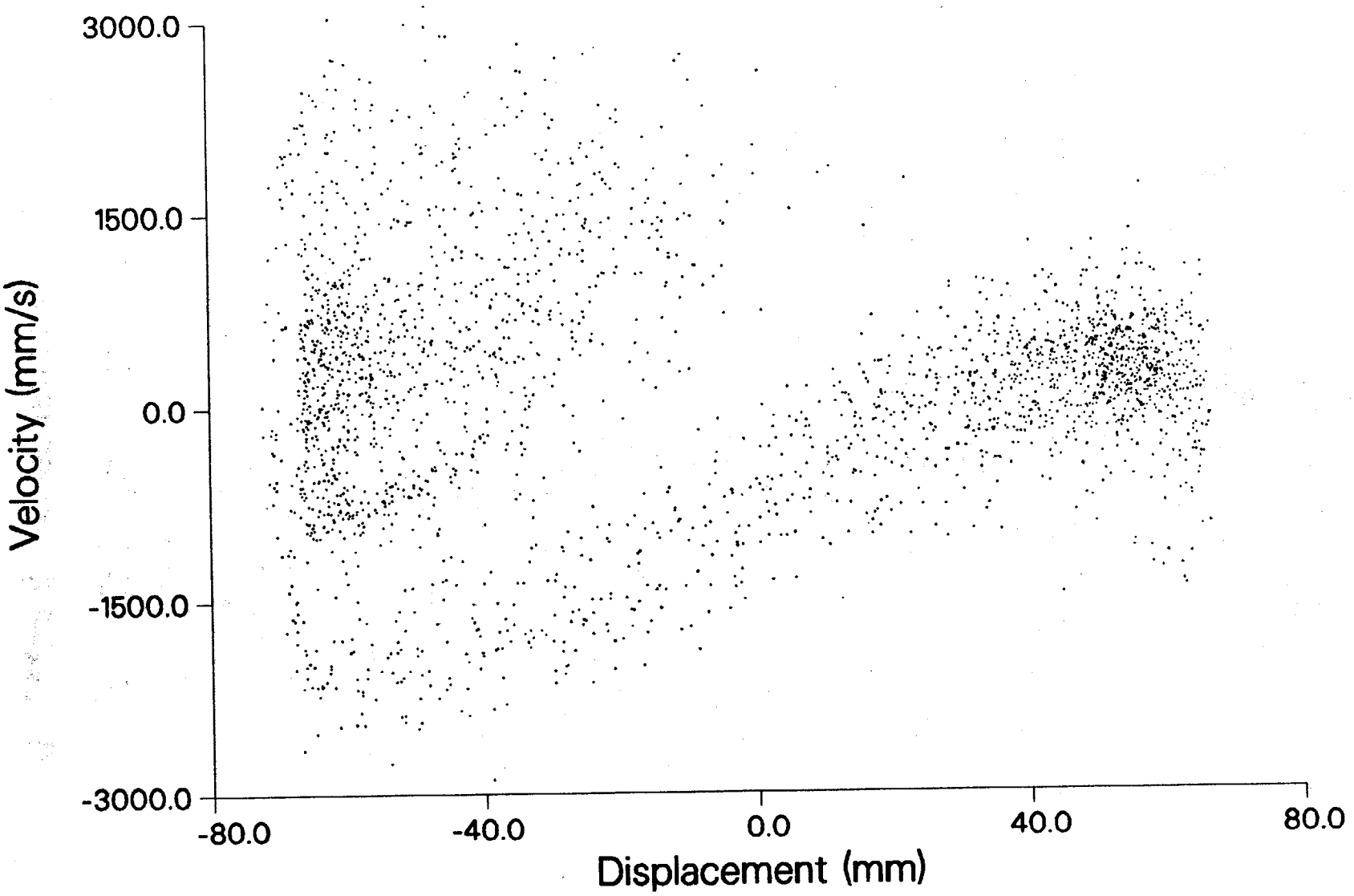

Fig. 5.2 Stroboscopic Poincare Plot of Simulated Chaotic Motion.

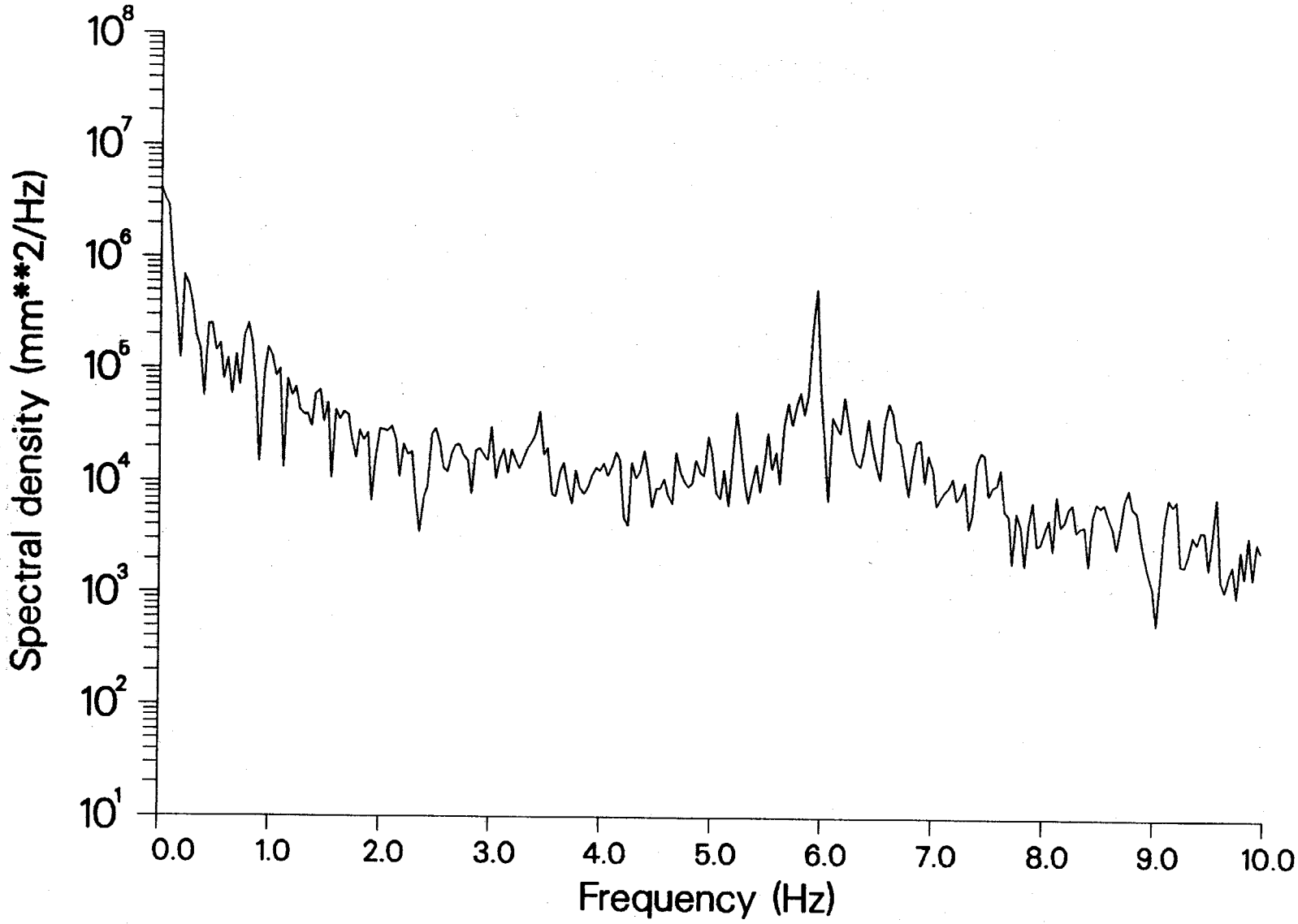

Fig. 5.3 Spectral Density Plot of Simulated Chaotic Motion.

NIST-114A
(REV. 3-89)

U.S. DEPARTMENT OF COMMERCE
NATIONAL INSTITUTE OF STANDARDS AND TECHNOLOGY

BIBLIOGRAPHIC DATA SHEET

1. PUBLICATION OR REPORT NUMBER
NIST/BSS-168

2. PERFORMING ORGANIZATION REPORT NUMBER

3. PUBLICATION DATE
February 1990

4. TITLE AND SUBTITLE

PERIODIC AND CHAOTIC MOTIONS OF A MODIFIED STOKER COLUMN: EXPERIMENTAL AND NUMERICAL RESULTS

5. AUTHOR(S)

Graham R. Cook and Emil Simiu

6. PERFORMING ORGANIZATION (IF JOINT OR OTHER THAN NIST, SEE INSTRUCTIONS)

U.S. DEPARTMENT OF COMMERCE
NATIONAL INSTITUTE OF STANDARDS AND TECHNOLOGY
GAITHERSBURG, MD 20899

7. CONTRACT/GRANT NUMBER

8. TYPE OF REPORT AND PERIOD COVERED
Final

9. SPONSORING ORGANIZATION NAME AND COMPLETE ADDRESS (STREET, CITY, STATE, ZIP)

National Institute of Standards and Technology (NIST)
Gaithersburg, MD 20899

10. SUPPLEMENTARY NOTES

[ ] DOCUMENT DESCRIBES A COMPUTER PROGRAM; SF-185, FIPS SOFTWARE SUMMARY, IS ATTACHED.

11. ABSTRACT (A 200-WORD OR LESS FACTUAL SUMMARY OF MOST SIGNIFICANT INFORMATION. IF DOCUMENT INCLUDES A SIGNIFICANT BIBLIOGRAPHY OR LITERATURE SURVEY, MENTION IT HERE.)

Records are presented of typical measured motion of a modified forced Stoker column, including periodic motion around a stable fixed point, periodic snap-through motion, and chaotic motion. Characterizations of the recorded chaotic motion include: the auto-correlation function; the spectral density plot; capacity dimensions;and the Lyapounov exponent. Two sets of numerical simulations were performed, in which the same spring stiffnesses (measured under static conditions) and the same dissipative forces (based on the viscous damping model) were used. The first set, in which the device was modeled as a multidegree of freedom system to account for the distributed mass and stiffness of the springs, yielded chaotic motions qualitatively similar to those recorded in the laboratory. No chaotic motions could be obtained from the second set, which did not reflect the fact that the spring properties are distributed and in which the device was therefore modeled as a one degree of freedom system. To the writers' knowledge, this is the first reported instance of an experimental structural system with continuous members for which a qualitatively successful simulation of the chaotic motion appears to necessitate the inclusion in the model of additional degrees of freedom to account for the effects of continuity.

12. KEY WORDS (6 TO 12 ENTRIES; ALPHABETICAL ORDER; CAPITALIZE ONLY PROPER NAMES; AND SEPARATE KEY WORDS BY SEMICOLONS)

Buckling; chaotic motion; dynamical systems; nonlinearity; structural dynamics; structural engineering; vibrations

13. AVAILABILITY

[X] UNLIMITED

[ ] FOR OFFICIAL DISTRIBUTION. DO NOT RELEASE TO NATIONAL TECHNICAL INFORMATION SERVICE (NTIS).

[X] ORDER FROM SUPERINTENDENT OF DOCUMENTS, U.S. GOVERNMENT PRINTING OFFICE, WASHINGTON, DC 20402.

[X] ORDER FROM NATIONAL TECHNICAL INFORMATION SERVICE (NTIS), SPRINGFIELD, VA 22161.

14. NUMBER OF PRINTED PAGES
44

15. PRICE

ELECTRONIC FORM